January 2001

CORONAL MAGNETOMETRY: A FEASIBILITY STUDY

P. G. Judge
R. Casini
S. Tomczyk
D. P. Edwards (ACD)
E. Francis (ACD)

HIGH ALTITUDE OBSERVATORY

NATIONAL CENTER FOR ATMOSPHERIC RESEARCH
BOULDER, COLORADO

CORONAL MAGNETOMETRY: A FEASIBILITY STUDY

P. G. Judge (HAO)
R. Casini (HAO)
S. Tomczyk (HAO)
D. P. Edwards (ACD)
E. Francis (ACD)

Contents

List of Figures

List of Tables

Acknowledgments

Abstract

Measurements of components of the vector magnetic field in the solar corona can potentially yield information critical to our understanding of coronal structure, dynamics and heating. In this report we re-examine various techniques for such measurements, in particular those that can be applied outside of active regions, to investigate issues critical to the development of a new "coronal magnetometer", and to lay down some foundations upon which a suitable instrument may be developed for synoptic observations.

The well-known forbidden coronal emission lines of magnetic dipole (M1) character appear to have the highest potential to address outstanding problems in coronal physics, especially those related to the storage and release of magnetic free energy. Measurements of the full Stokes vector of M1 lines can constrain *both* the line-of-sight (LOS) field strength, $B_\parallel$, through the **longitudinal Zeeman effect** seen in Stokes V profiles, *and* the direction of the vector field projected onto the plane-of-the-sky (POS), through the analysis of **resonance scattering**-induced linear polarization seen in Stokes Q and U, in the so-called "strong field" regime of the Hanle effect. Such measurements can, coupled with additional data and models, reveal information on coronal magnetic fields, potentially including current systems, unobtainable by other means available now or in the near future.

Measuring the weak, Zeeman-induced Stokes V signal presents the greatest observational challenge. Recent work at the NSO Evans coronagraph succeeded in detecting convincingly the Zeeman V signal in Fe XIII 1.0746 μm (Lin et al. 2000). A more dedicated instrument designed to detect this effect from the outset will have (in principle) little trouble in measuring the linearly polarized signal from the resonance scattering process. The major obstacle is to account for cross-talk in V induced by the dominant (by a factor of 10^2) linear polarization signal.

Both effects can in principle be studied with a single coronagraphic instrument. Based upon simulations of the Stokes profiles, we argue that any new instrument must be able to measure $\frac{V}{I}$ profiles to 1 part in 10^4, and it should span wavelengths from 1.0746 μm (the wavelength of a line of Fe XIII) with capability extending ultimately to 4 μm (to include lines of Mg VIII and Si IX), and down to 0.5303 μm (Fe XIV). This wavelength range points to a reflecting coronagraph. We argue that first priority should be given to build a spectro-polarimeter that includes the 1.0746, 1.0798 μm M1 lines of Fe XIII, the permitted He I lines near 1.0830 μm, and perhaps the Fe XIV 0.5303 μm line in a higher spectral order, keeping longer wavelength capability as a secondary goal. The He I 1.0830 μm line can in principle be used to determine vector magnetic fields through the Hanle effect in prominence fields with $|\vec{B}| \sim 1$ Gauss, and to determine the LOS strength and POS field direction in the "strong field" regime expected in prominences with stronger fields.

Abbreviations/notations/units: LOS: line of sight; POS: plane of sky; M1: magnetic dipole; E1: electric dipole; E2: electric quadrupole; F-corona: Fraunhofer (dust-scattering) Corona; K-corona: Continuum (electron-scattering) corona; E-corona: emission-line corona; longitudinal magnetic field: component of the field parallel to the field vector; transverse magnetic field: components in a plane normal to the field vector; by "resonance polarization" we refer to the restricted case of resonance scattering in the "strong field" regime, see page 18; Notation- [Fe XIV] means a forbidden line ("[ ]") in the 14th spectrum (i.e. the ion Fe^{13+}) of iron. "Red line": [Fe X 0.6374] μm; "Green line": [Fe XIV] 0.5303 μm. All wavelengths are given in air, in units of microns (μm). CGS units are otherwise used throughout.

> **Critical points are emphasized throughout the text in a "shadowed frame", like the one around this sentence.**

1   Introduction

1.1   Motivations

Magnetic fields emerging from beneath the solar photosphere, buffeted by convective motions, control the forcing and heating of the solar corona. Away from relatively strong fields associated with active regions, few useful measurements of coronal magnetic fields exist, because they are so difficult to make. Synoptic measurements of the line-of-sight (LOS) components of the photospheric field strength, $B_\parallel$, and filling factor yield average field strengths of between 3 and 13 Gauss[1], depending on the phase of the solar-activity cycle (e.g., Schrijver and Harvey 1994). These values are broadly compatible with available extrapolations from measured field strengths in the solar wind (Section 1.3).

If even relatively crude constraints on components of the coronal vector magnetic field could be obtained – as might be provided through maps of linearly and circularly polarized light in forbidden lines (e.g., see Figure 17 on page 50)– several important questions could be addressed. For example:

- What is the relationship between "plasma loops", i.e. those observed in maps of emission line intensities, and the actual magnetic field? Is there a one-to-one correspondence between "magnetic loops" and "plasma loops"? The observed plasma loops are generally believed to trace out particular magnetic lines of force within a coronal volume that is filled with magnetic field, force balance dictating that the field strength be weaker in the plasma loops than in the neighboring, "invisible" parts of the corona. But it is also possible that (some of) these could instead be current sheets (e.g., Fort and Martres 1974, Klimchuk et al. 1992), delineating instead what appear to be "loops" of electrical current or "separators" which are ribbons of current flow (Longcope 1996).

- What kinds of magnetic configurations lead to the launch of coronal mass ejections (CMEs)?

- How good (or bad) are specific MHD models of large scale coronal structures ($\sim$ 500 Mm characteristic length scales), such as those for prominence cavities and helmet streamers (as discussed by Low 1994, for example)? (Prominences themselves can provide additional information on the magnetic field: see section 1.4 and section A.4 which is found in the Appendix, page 59).

- What is the basic structure of smaller-scale features such as polar plumes and active-region loops (e.g. Figure 4) on $\sim$ 100 Mm characteristic length scales?

- What is the nature of the change in coronal magnetic structure that accompanies the 11-year solar cycle's switch of magnetic polarity?

With maturity, a synoptic coronal magnetometry observing program, in cooperation with photospheric magnetometers, might also be expected to yield answers to more challenging questions. For example, how good are field extrapolations (Section 1.5) based upon vector-field measurements in the photosphere, in a variety of structures? What can we learn from discrepancies between extrapolated and measured magnetic fields? What can we learn about the nature of current systems in the corona, and the physical state of the magnetic structure in

---

[1]These numbers should probably be considered as upper limits to the coronal field strengths: some of the measured photospheric flux returns to the photosphere before it can rise to coronal heights. Also the field strengths in quiet regions will be less than these average values.

the corona as it responds to injection of magnetic energy from below? Can one develop techniques for predicting the probability that CME's will be launched from a given set of coronal and/or photospheric magnetic field measurements? Can one develop techniques for predicting the probability that flares will occur? Can such data allow us to put meaningful constraints on the nature of the coronal heating mechanism(s)?

1.2 Purpose

> **The purpose of this report is:**
> • **To review techniques for measuring properties of coronal magnetic fields.**
> • **To identify the most promising technique.**
> • **To provide enough information to develop an instrument and identify the kind of site/platform needed for its successful operation.**

To anticipate the difficulty of some issues discussed below, we end this Section with a quote, from Jack Harvey's Ph.D. thesis (Harvey 1969). He tried to use the (longitudinal) Zeeman effect to determine LOS coronal field strengths using the Green coronal line ([Fe XIV] at 0.5303 μm), the brightest of the visible forbidden coronal lines:

> "We will consider the Zeeman effect on increasing scales of resolution: atomic to observational. Problems to thwart the investigator occur on all scales of resolution."

While the atomic problems have since been mostly resolved (as discussed below), we will see that the observational problems identified 30 years ago by Harvey remain, but that they are mitigated by the better instrumentation available now, thus presenting us with an opportunity for significant progress.

1.3 Physical properties of the corona

Before proceeding it is prudent to review some basic properties of the solar corona. Table 1 lists typical physical conditions present in the low corona (less than $\approx 0.4 R_\odot$ above the photosphere) in the quiet Sun. The low corona is a hot tenuous plasma permeated by magnetic fields with energy densities up to 100 times larger than the plasma's thermal energy density ("low-β"). The mean free paths of dominant particles (electrons and protons) are less than some important macroscopic scales (lengths of loops, pressure scale heights). The largest scales may therefore be treated in the magnetohydrodynamic regime. The plasma is highly electrically conducting and the plasma can be considered to be frozen into the field lines. The corona is also highly thermally conducting- electrons can rapidly transport energy along field lines. Across the field lines it is far less conductive. Transport processes are therefore highly anisotropic.

Under the thermodynamic conditions listed in Table 1, the emission line coronal spectrum is dominated by ions of the third row of the Periodic Table that are between roughly 7 and 13 times ionized (Edlén 1943). The high temperatures and low densities imply that the Sun's corona emits spectral line radiation very inefficiently in the most abundant chemical species

Table 1: typical conditions at the quiet Sun's coronal base

	Physical quantity	Units	value
Magnetic and thermal Properties			
	T_e electron temperature	K	10^6
	P_e electron pressure	cm^{-3} K	3×10^{14}
	N_e electron density	cm^{-3}	3×10^8
	ρ mass density	g cm^{-3}	5×10^{-8}
	c_S sound speed	km s^{-1}	100
	$|B|$ typical field strength	G	$1 \rightarrow 10$
	β $(P_{\mathrm{plasma}}/\frac{B^2}{8\pi})$		$10^{-2} \rightarrow\lesssim 1$
	c_A Alfvén speed $\sqrt{\frac{B^2}{4\pi\rho}}$	km s^{-1}	$100 \rightarrow 1000$
	$q_\parallel$ heat flux, parallel to $\vec{B}$	erg cm^{-2} s^{-1}	$\kappa_\parallel T^{5/2}\nabla T$
	$\kappa_\parallel$	erg cm^{-1} K$^{-7/2}$ sec^{-1}	2×10^{-6}
	ν_e electron gyro freq.	Hz	$3 \times 10^{6\rightarrow7}$
	ν_p proton gyro freq.	Hz	$1.5 \times 10^{3\rightarrow4}$
	τ_{ee} electron self collision time	s	0.05
	τ_{pp} proton self collision time	s	2
	$\nu_e \cdot \tau_{ee}$		$1.5 \times 10^{5\rightarrow6}$
	$\nu_p \cdot \tau_{pp}$		$3 \times 10^{3\rightarrow4}$
	$\lambda = v \cdot \tau$ (mean free path)	cm	10^8
	$\kappa_\perp/\kappa_\parallel$ [a]		$(2\pi\nu\tau)^{-2}$
	ν_{pe} electron plasma freq.	Hz	1.5×10^8
"Closed" (loop) structures			
	Loop length L	cm	5×10^9
	R_m mag. Reynolds num.		$\gg 1$
	$\nabla \cdot F_{RAD}$	erg cm^{-3} s^{-1}	2×10^{-5}
	$\nabla \cdot F_C$	erg cm^{-3} s^{-1}	2×10^{-3}
	L/c_S	sec	10^2
	L/c_A	sec	$10^{1\rightarrow2}$
	Rad. time scale	sec	3×10^3
	Cond. time scale	sec	2×10^2
"Open" (wind) structures			
	Pressure scale height H	cm	2×10^9

Note: These are typical values: significant fluctuations exist (especially in the thermal conditions). Two values are listed for magnetic field strengths of 1 and 10 Gauss, for certain parameters. Such values are delimited by use of an arrow ("$\rightarrow$"). Note that ν is used to denote frequency (not angular frequency) in the above Table. *a*: this is valid in the limit $2\pi\nu\tau \gg 1$.

(hydrogen, helium), because these are almost fully ionized. The spectral line radiative signatures are predominantly from lines of trace species, such as iron. Thermally emitted continuum radiation from the corona is dominated by Bremsstrahlung radiation from free electrons. It is strong only at X-ray and radio wavelengths, where respectively the emission coefficients and the optical thicknesses become large. Last, but not least, Thomson scattering of photospheric light by coronal electrons is the dominant contributor to the continuum emission ("K-corona") low in the corona, at visible and near infrared wavelengths.

It should be re-emphasized that these conditions apply to the low corona, i.e. just a few pressure scale heights above the photosphere (i.e. below say $0.4R_\odot$). Conditions change substantially higher in the corona, where the solar wind kinetic energy density begins to dominate the magnetic energy density at 20-30 or so solar radii, and the plasma moves from the collisional
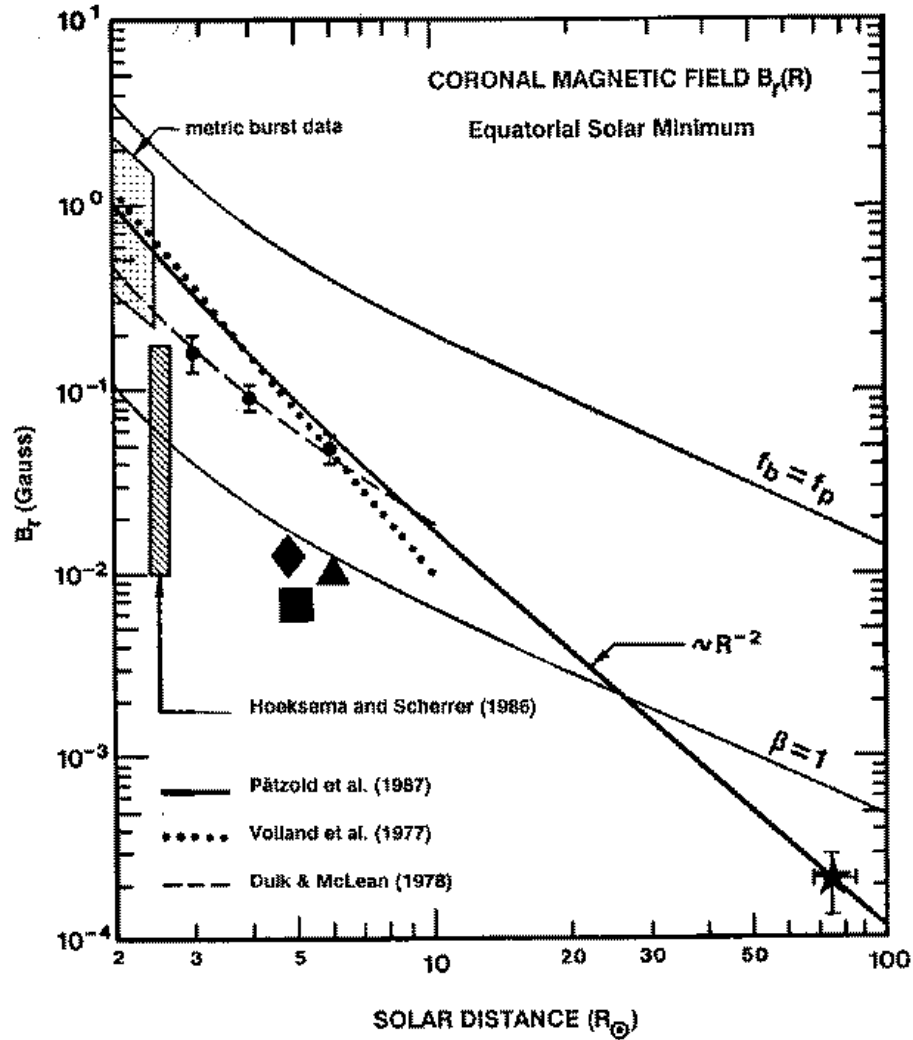
Figure 1: Coronal magnetic field strength as a function of solar distance, from Bird and Edenhofer (1990) (the Figure is taken from this review). The Figure illustrates, *anno 1990*, not only the expected magnitude of field strength but also something of the nature of the radio and extrapolation techniques that have been used to determine it (see text).

to the collisionless regime. Knowledge of the radial dependence of the magnetic field strength at such large heliocentric distances, *anno 1990*, is summarized in Figure 1, taken from Bird and Edenhofer (1990). The Figure represents a compilation of measurements and other constraints on the field strength as a function of heliocentric radius, from a wide variety of conditions in the Sun, including both open and closed field regions (Dulk and McLean 1978). Between 1.02 and $10R_\odot$ Dulk and McLean (1978) give the following empirical formula, based upon a variety of observations, for the magnitude of the magnetic field:

$$B = \frac{1}{2}\left(\frac{R}{R_\odot} - 1\right)^{-3/2} \quad \text{G}, \tag{1}$$

shown as the dashed line in Figure 1. Of the other observations shown in the Figure, we note that

the curve marked "$f_B = f_p$" is simply that where the electron gyrofrequency equals the plasma frequency (assuming that the electron density varies roughly as R^{-2}), representing an upper limit (otherwise fundamental mode gyroresonant emission would be present, which contradicts most observations). The hatched bar marked "Hoeksema and Scherrer 1986" in Figure 1 shows potential field extrapolations based upon photospheric measurements (Hoeksema and Scherrer 1986). Bird and Edenhofer (1990) noted that a fraction of these extrapolations yield field strengths that lie below the $\beta = 1$ contour, which, with other Faraday rotation measurements, indicated a significant discrepancy. This point and the remaining observations shown in the figure are discussed in detail in Bird and Edenhofer (1990).

1.4   Methods for determination of coronal magnetic fields

In this Section we briefly discuss the relative merits of all techniques that are available for the determination of properties of the magnetic field in the quiet corona, i.e. which are capable of detecting field strengths of only a few Gauss. The reader can refer to the Appendix for more details. Table 2 lists nine potentially useful methods mentioned in the Appendix for the determination of properties of the coronal magnetic field. All remote-sensing techniques rely on measurements of the state of polarization of light, traditionally described by the "Stokes vector" $\mathbf{S} \equiv (I, Q, U, V)^T$ (e.g., Shurcliff 1962).

> **Based upon several criteria, not least of which is the ability of the techniques to answer the questions listed in Section 1.1, we will argue that *spectropolarimetry of M1 (forbidden) coronal emission lines (particularly in the infrared) is worthy of serious consideration for the development of a coronal magnetometer.* This is not to the exclusion of other methods, but it does appear to provide the best opportunity for addressing the important problems outlined in Section 1.1 in the forseeable future.**

First, we note that to address properly the questions raised above, we must be able to make measurements which sample (with sufficient angular resolution) volumes of space comparable to the solar volume. Many of the problems posed above require measurements as close as possible to the solar surface, for example to determine the nature of polar plumes, active regions, and the relationship between magnetic fields and plasma loops. Furthermore, we must be able to follow the evolution of such measurements with time.

A glance at Table 2 shows that we can immediately discount **direct magnetometer measurements**, as a primary tool. **Faraday rotation** measurements yield path integrated averages only along lines of sight to specific polarized radio sources. The occultations occur infrequently, and in any case two-dimensional mapping is impossible. Such measurements would not allow us to address the kinds of problems mentioned above. There are similar problems with using the unusual conditions encountered in comet tails (see the Appendix, Section A.4).

Of the remaining six methods, two are limited through special physical conditions that must exist in order to apply the methods in the first place. The first concerns active regions, which have large field strengths (> 100 Gauss in the coronal plasma itself). These can and have been

Table 2: Techniques for determining coronal magnetic fields

Technique	Measured Quantity	Derived	Proven?	Notes
Direct magnetometry (in situ spacecraft)	Induced currents (Faraday's Law)	$\vec{B}$	Y[a]	$> 62 R_\odot$ to date $\gtrsim 4 R_\odot$ in principle
Faraday Rotation of cosmic radio sources	Rotation of plane of polarization	$\int \vert n B_\parallel \vert dl$	Y[b]	special LOS only
Modified Bremsstrahlung	Polarized radio waves	$B_\parallel$	Y[c]	All regions
Gyroresonant emission	Polarized radio waves	$\vert \vec{B} \vert$	Y[d]	Active regions
Hanle effect in H Lyman α O VI 1032	Line depolarization, rotation	$\vec{B}$	N[e]	UV ($\Rightarrow$ space) coronagraph
Longitudinal Zeeman effect (M1 lines, e.g. [Fe XIV] 0.5303 μm)	Circularly polarized lines	$B_\parallel$	Y[f]	Eclipse/ coronagraph
Resonance Polarization[†] (M1 lines, e.g. [Fe XIV] 0.5303 μm)	Linearly polarized lines	POS direction	Y[g]	Eclipse/ coronagraph
Zeeman, Hanle effect in cometary tails	Full stokes polarimetry	$\vec{B}$	N	Tied to orbit, night, or or coronagraph
Hanle effect (permitted lines, e.g. H α, He I 1.083 μm)	Line depolarization, rotation	$\vec{B}$	Y[h]	Cool plasmas (prominences)

[†]In this report we use this term to refer to the restricted case of resonance scattering in the "strong field" regime discussed on page 18. *a.* Many spacecraft have measured the magnetic field in the heliosphere, for example the *Helios* spacecraft (Mariani and Neubauer 1990) which made measurements as close as $62 R_\odot$. *b.* See, e.g., Bird and Edenhofer (1990) *c.* See e.g., Gelfreikh (1994). *d.* A large literature exists on this topic, e.g., see Bastian (1995). *e.* Bommier and Sahal-Bréchot (1982), Sahal-Bréchot et al. (1986), probably limited to $R < 2 R_\odot$ since the Hanle sensitive regime is where $\vert \vec{B} \vert \approx 10$ G. *f.* Lin et al. (2000). *g.* See e.g., Arnaud and Newkirk Jr. (1987). *h.* e.g., Landi Degl'Innocenti (1982), Leroy (1989).

effectively studied through **gyroresonant emission** at radio wavelengths. The second special circumstance involves plasma that is at coronal heights, but is anomalously cool: prominence plasmas radiate permitted lines from IR to UV wavelengths with polarization signatures that can yield information on the vector magnetic field through the **Hanle effect**. This effect involves both depolarization and rotation of linearly polarized light originally generated by anisotropic processes. In the case of prominences, the linear polarization originates from irradiation of the prominence by anisotropic light originating from the solar disk. While we believe that such measurements can and should be used, we discount these two methods as *primary* tools for the development of a synoptic instrument which can address the problems outlined above, because of the special physical conditions under which the techniques can be applied.

Of the four remaining techniques, the **modified Bremsstrahlung** method applied at radio wavelengths has yielded useful information on the LOS magnetic field strength. The method

is currently limited by lack of adequate spatial resolution, the problem of knowing the height of formation of the radio emission, and the dependence of the analysis on underlying assumptions concerning the thermal structure of the corona. It is fundamentally limited to the LOS component– no other information can be obtained from such measurements– even in principle.

The **resonance polarization** technique[2] has yielded useful information on the direction of coronal fields in the POS. There remain two diagnostics of the million degree coronal plasma's magnetic field that have not yet been proven useful. The first is again the **Hanle effect**, but applied to emission from atoms/ions in the coronal (10^6K) plasma proper. Owing to the large abundance of hydrogen, and the fact that sufficient emission is created even at coronal temperatures, the Lyman α line appears to hold the most promise (e.g., Bommier and Sahal-Bréchot 1982, Fineschi et al. 1993). The second is the **longitudinal Zeeman effect**, which can yield information on the LOS field strength (Harvey 1969, Kuhn 1995). The Hanle effect, as applied to H Lyman α, suffers from the disadvantage that a complete quantum theory to attack the problem of frequency-dependent resonance scattering including quantum coherences between sub-levels is still under development. Furthermore, such work would have to be performed from a **space-based platform, a feasible but expensive option**. Current designs have adopted external occulters which limit observations to heights $> 0.8R_\odot$ above the solar limb, although $0.3R_\odot$ appears to be feasible (Fineschi, private communication 2001). This method, while potentially very powerful, is not likely to produce results in the next few years, given the time needed to develop and fly a new space based instrument. Furthermore, it is not able to see features very low in the corona.

The longitudinal Zeeman effect has suffered from the disadvantage that very high precision differential measurements are needed to detect the small Stokes V signals. Only recently, Lin et al. (2000) conducted a proof-of-concept experiment. They detected the longitudinal Zeeman V signal in line 1.0746μm of Fe XIII with a non-dedicated instrument. This experiment showed that linear polarization cross-talk on V from the stronger resonance-scattering polarization signal represents the major difficulty for sensitive measurement of the coronal field strength.

Keeping in mind the motivations listed in Section 1.1, we are left with the three techniques, emphasized in **bold faced** type, listed in Table 2, as the most promising methods for obtaining routine measurements of components of the coronal magnetic field. Of these, both the longitudinal Zeeman effect and resonance polarization signals can be observed with the same spectral lines, and the same instrument. Forbidden emission line measurements can yield constraints on both the LOS field strength and POS direction. Radio techniques can yield just the former. The POS field direction measurements will in principle prove important in two ways. First, the relationship between "plasma loops", seen in intensity data in coronagraphs and at EUV wavelengths, and the underlying magnetic field configurations can be addressed. Second, the data can potentially be used to constrain magnetic free energy in the corona, because some constraints on the *curl* of the magnetic field can be set, at least in principle.

The forbidden line techniques are only partially explored, but hold substantial promise. Therefore we focus next on forbidden emission lines from typical coronal ions (the dominant lines of the "E-corona"). We will examine these lines as diagnostics of the magnetic field through application of the two methods together, with the aim of helping to determine some constraints for the development of a single coronagraphic instrument devoted to measuring these effects. Before proceeding we re-emphasize the obvious fact that, because of the enormous solar disk intensities at visible and near-infrared wavelengths, these forbidden line methods require *eclipse or coronagraphic* observations. Thus, **these techniques can probably never be used to**

---

[2]In this report we use this term to refer to the restricted case of resonance scattering in the "strong field" regime discussed on page 18.

observe the coronal plasma emitting on the solar disk. The **only** techniques that show promise in this regard are the radio methods, or the Hanle effect applied to filaments (prominence plasma seen on the disk, e.g. Lin et al. 1998), each with their own limitations.

1.5   Field extrapolations: Why measurements are needed instead

The discussion thus far has addressed techniques that exploit remotely sensed or *in situ* properties of the coronal plasma or magnetic field itself. Yet considerable efforts have been made by many authors to determine the coronal fields via extrapolation procedures based upon data measured either at the photosphere or in the solar wind (e.g. see the recent work of Gibson et al. 1999, Amari et al. 1999, Linker et al. 1999). As stated above, one goal of a magnetometry project is to test existing extrapolation techniques. We must therefore look more carefully at why measurements of the magnetic fields in coronal plasma itself, and not extrapolations from the photosphere or heliosphere, are highly desirable.

Magnetic field extrapolation from remotely sensed photospheric data is a risky proposition for two fundamental reasons. First, the extrapolated fields are sensitive to errors in the boundary conditions (the problem is poorly posed), such as the observational errors that arise when measuring vector magnetic fields in the photosphere (Low and Lou 1990). Second, the corona's response to footpoint motions in the lower atmosphere is to relax to a state that includes current systems that, because the MHD force balance is non-linear, cannot easily be determined theoretically or even uniquely (e.g., Parker 1994). The presence of such currents makes meaningful extrapolations difficult, if not impossible. For example, analyses of some radio data have already revealed evidence that magnetic fields in the corona over some active regions cannot be characterized by a "constant-α" (curl $\vec{B} = \alpha\vec{B}$) force-free state (White 2001), which is an approximation commonly used.

The problem of field extrapolation downwards from *in situ* measurements of $\vec{B}$ from spacecraft in practice is limited because existing data have been obtained down to just $\approx 62R_\odot$ (from the *Helios* spacecraft). This radial distance exceeds both the trans-sonic and trans-Alfvénic points in the wind flow. Thus, such measurements can be viewed as providing boundary conditions on a physical system that must be carefully modeled to extract information on fields closer to the Sun (as done for a dipolar magnetic source by Pneuman and Kopp 1971, for example). One interpretation of Figure 1 is that existing measurements at $\geq 62R_\odot$ show order of magnitude confirmation of field strengths determined remotely via other techniques. Future spacecraft will improve the situation (e.g. the Solar Probe, Solar Orbiter missions) but will orbit close to the Sun only briefly. Nevertheless, a close fly-by of a spacecraft carrying magnetometers affords a very special opportunity for coronal physics that should be fully exploited.

Aside from these important problems, measurements (and not extrapolations) are needed to address the particular questions listed in Section 1.1.

2   Forbidden Lines As Diagnostics Of The Coronal Magnetic field

Henceforth we will focus almost exclusively on forbidden emission lines. These are magnetic dipole (M1) transitions between levels of ground terms of ions of abundant elements of the third and fourth rows of the Periodic Table of elements. Furthermore, we will (for a while) restrict our attention to the longitudinal Zeeman effect, because any instrument capable of measuring the longitudinal Zeeman effect will have ample capability of measuring the resonance polarization once cross-talk problems are solved (Section 1.4). We believe that routine measurements of the longitudinal Zeeman effect in the corona will be achieved in the near future, because:

- The magnitudes of the Stokes V profiles vary in proportion to the wavelength λ of the transition, all other parameters being equal. Several infrared lines have been recently computed to be bright enough for this kind of work (Judge 1998). A promising line of Si IX (at 3.9346 μm) has recently been detected (Kuhn et al. 1999), albeit marginally.

- Current IR detectors are dramatically improved over those used in earlier work. Recent data are limited by background sources and not instrumental effects which often limited data acquired in the 1960s and 1970s. Large 2D detector arrays (e.g., 1024×1024 pixels) are being developed, compared with the handful of diodes used earlier (e.g., Querfeld 1977), which have obvious advantages for improving cadence, field-of-view, and spectral performance.

- Background scattered light intensities and seeing problems are substantially reduced at IR wavelengths.

- Reflecting coronagraphs are under development (Smartt and Koutchmy 1995, Moretto and Kuhn 1999), thereby avoiding chromatic and transmission problems with existing refracting coronagraphs.

2.1   A brief history of forbidden line spectroscopy

Spectroscopy of the Sun's corona at visible wavelengths has been a continuing research area, especially since Edlén (1943), building on work by Grotrian, uncovered the nature of the unidentified lines in the coronal spectrum. A brief but nice review of the corona seen in emission lines, the "E-corona", is given by Bray et al. (1991), although with an emphasis on closed field regions. Some significant milestones in this area include:

1869: Young and Harkness observed visually the Green coronal line during eclipse, with a spectrograph.

Late 1800s: Young noted that gross mass motions in the corona, as seen in Doppler shifts of the Green line, was much less than in prominences.

1930's: Lyot (1930) developed the coronagraph and narrow band filters, and used a spectrograph to obtain coronagraphic spectra (for wavelengths below 1.35 μm). This helped to set the stage for Edlén's work. Lyot found many unidentified lines, including those at 1.0746 and 1.0798 μm (Lyot 1939).

1937: Lyot (1935) suggested that the width of the Green line might be due to thermal motions.

1939: Grotrian (1939) proposed tentative identifications for the Red coronal line (Fe X) and a line at 789.2 nm (Fe XI).

1943: Edlén (1943), following Grotrian, identified 4 lines against laboratory measurements, and many other lines using isoelectronic extrapolation (0.33 - 1.0797μm) with 9-14 times charged ions. This paper marks perhaps the beginning of modern coronal physics.

1940s–1960s: Several coronagraphs were developed (Climax Colorado, Pic-du-Midi France, Arosa Switzerland, Sacramento Peak New Mexico, Haleakala Hawaii, for example) for the measurement of coronal thermal properties, without diagnosis of the coronal magnetic field. Many lines at visible wavelengths were identified as forbidden lines in highly ionized ions. The two brightest visible lines were examined extensively: the Fe X 0.6374 μm Red line and the Fe XIV 0.5303 μm Green line.

1964: Burgess (1964) largely reconciled temperatures derived from ionization equilibrium with those derived from forbidden line widths through invoking di-electronic recombination, a process which had previously been missing from earlier studies.

1965: Billings (1965) published his book concerning the coronal spectrum. Several aspects of the data are important here: the K-corona and E-corona are qualitatively different; even Red and Green line images are different; line profiles revealed subsonic non-thermal motions (linewidths) and small subsonic flows (lineshifts).

1965: Charvin (1965) (see also Hyder 1965, Perche 1965a, 1965b) showed how M1 lines are influenced by anisotropic irradiation, and how measurements of the linear polarization of these lines can be related to the direction of the magnetic field projected onto the POS. This marks the birth period of the "resonance polarization" method.

1966/1967: Münch (1966) followed early work by Swings (1944) with theoretical estimates of forbidden coronal **infrared** line intensities. With colleagues, he made comparisons with photoelectric PbS detector data (1-3 μm) from the 1966 eclipse (Münch et al. 1967).

1969: At Climax, Colorado, Harvey (1969) used the longitudinal Zeeman effect to determine LOS fields in coronal structures. Most detections were made in prominences using cool lines of weakly ionized atomic species. In the corona proper, he measured Stokes V profiles of [Fe XIV] 0.5303 μm across the line profile, using photographic and photoelectric detectors. Although he made careful measurements, the data were (by today's standards) relatively noisy, and he obtained no convincing detections in coronal (million degree) plasma.

Table 5-13

Measurements of coronal magnetic fields

Date (1967)	Time (UT)	PA (°)	Aperture (arc-sec)	B$_{||}$ (gauss)	Nearby B$_{||}$ (gauss)
VII-3	1646-1716	73	30 x 60	13±20	+
VII-19	1539-1644	119	30 x 60	- 6± 4	-
VIII-11	1527-1607	58	30 x 60	- 2± 8	-
VIII-12	1543-1603	113	30 x 60	- 1± 5	-
IX-2	1551-1618	294	30 x 60	0± 7	-3.6±.3
X-12	1605-1633	304	14 x 356	-1.5±.5	-4.0±.7
(1968)					
I-21	1713-1815	110	15 x 330	-2.0±.7	-

Table 3: Table listing the results of Harvey's attempts to measure coronal field strengths via the **longitudinal Zeeman effect** in forbidden coronal emission lines. These data were obtained using the Green line, observed from Climax Colorado. From Harvey (1969).

1971: Olsen et al. (1971) detected several other lines between 1 and 3 μm during eclipse using an aircraft-borne Fourier Transform Spectrometer (FTS) with faster solid state detectors than used by Münch et al. (1967).

1970's/1980's: This period saw the advent of diagnostics of the orientation of $\vec{B}$ projected onto the POS, through the development of the theory of Stokes Q, U profiles (the "resonance polarization" method). Sahal-Bréchot (1974, 1977) expanded the earlier theory of Charvin, Hyder and Perche to include (thermal, hence isotropic) collisional processes. for the [Fe XIV] 0.5303 μm and [Fe XIII] 1.0746 μm forbidden lines. In parallel, similar theoretical modeling of [Fe XIII] 1.0746 μm was performed by House (1977).

1970's/1980's: Polarimetric coronagraphs were developed to measure solar Q, U profiles of M1 emission lines. HAO/NSO's *"KELP"* ("K-corona and Emission Line Polarimeter"[3]) instrument (e.g., Querfeld and Smartt 1984, Arnaud and Newkirk Jr. 1987) measured the Fe XIII 1.0746 μm line, with successful determinations of the orientation of the magnetic field, projected onto the plane of the sky. Similar data and results were obtained at Pic du Midi, but using instead the [Fe XIV] 0.5303 μm line (e.g., Arnaud 1982).

Early 1990's: Infrared detectors with very deep wells were applied to coronal studies (Penn and Kuhn 1994, Kuhn et al. 1996), whose data are limited by background emission and not instrumental effects. Earlier infrared measurements (from the 1960's and 1970's) appeared to be "optimistic": they may have over-estimated line intensities.

1995: Kuhn (1995) derived an upper limit of 40 Gauss from the longitudinal Zeeman effect in the infrared [Fe XIII] line at 1.0746 μm, using the Evans coronagraph and a good, but not state-of-the-art, detector. He concluded that *potentially one can do much better, by using a more suitable telescope, better detectors (already available), and perhaps selecting more sensitive lines (further into the infrared)*.

---

[3]Not to be confused with "CELP" which stands for "coronal emission line polarization".

1998: Prompted by Kuhn's (1995) work, Judge (1998) investigated atomic term systems and made theoretical intensity calculations, to try to identify the strongest forbidden transitions in unexplored infrared regions. The ion Si IX has a line at 3.9346 μm that is expected to be particularly strong. Figure 2 shows calculated intensities of optical and infrared forbidden lines, as would be seen from a vantage point above the earth's atmosphere, based upon a representative thermal model of the corona.

1998: Kuhn et al. (1999) detected excess IR emission near 3.93 μm in a small aperture filter experiment run during the 1998, 26 February eclipse from an airborne platform. While not a definitive result by itself (an integration time of just a few seconds was used), the marginal (2σ) "detection" of the Si IX line expected near 3.9346 μm was consistent with data of EUV lines of Si IX from the CDS instrument on SOHO, based upon the calculations. This line is therefore potentially a valuable diagnostic for application of the longitudinal Zeeman effect. Figure 3 shows the results of this experiment.

1999: Casini and Judge (1999) developed the quantum theory for the formation of all four Stokes parameters of M1 emission lines, extending the work from the 1960's and 1970's to include Stokes V. Only the formalism for particle collisions remains to be completed.

1999: Lin, Penn, and Tomczyk detected the V polarization signature of Fe XIII 1.0746 μm with a S/N of 30 or so. A similar effort by C. Keller and collaborators using the Fe XIV 0.5303 μm line, and a very different focal plane package (Stenflo and Keller 1997) at the same instrument, failed to detect the effect (Stenflo, private communication 1999).
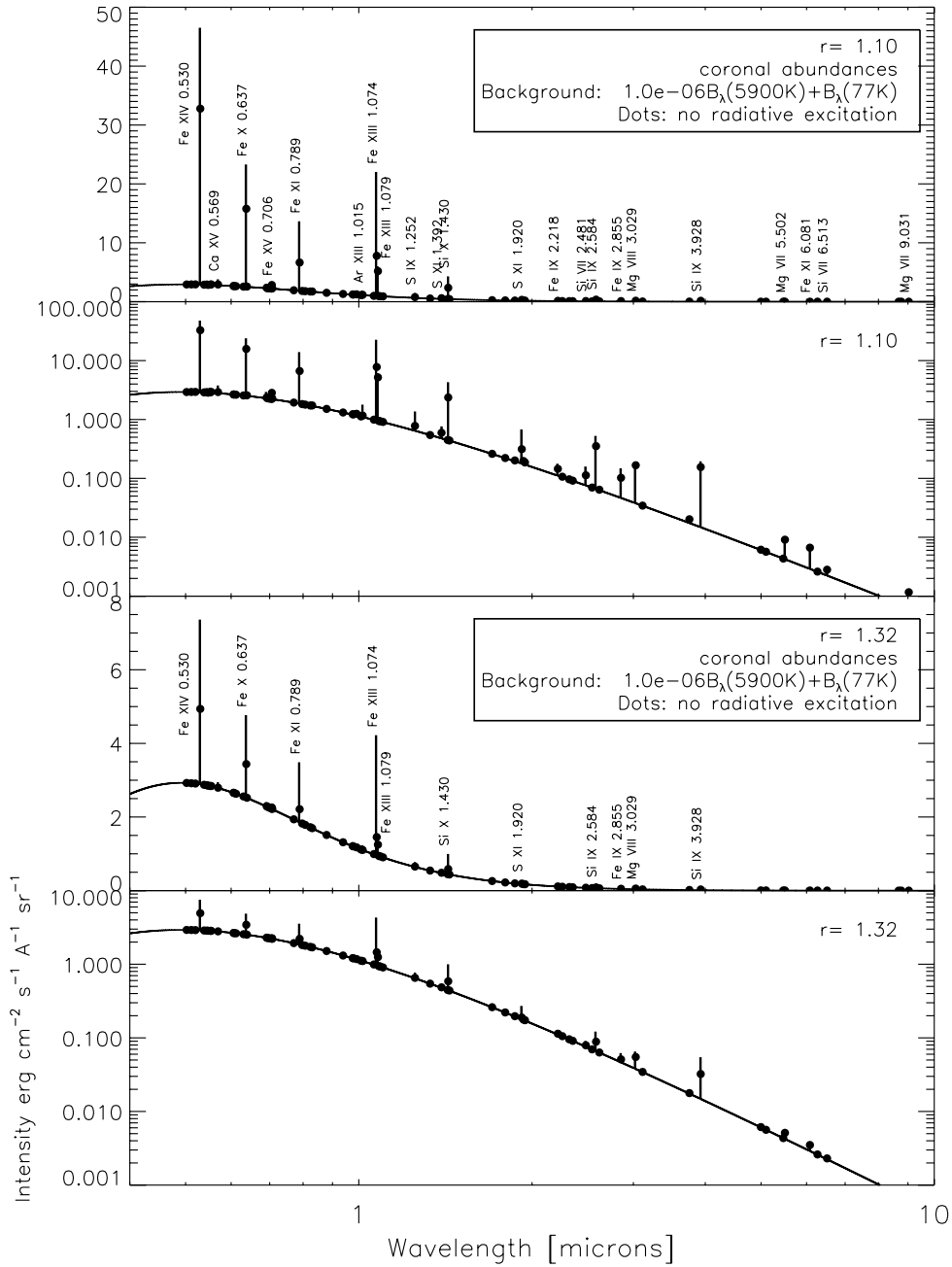
Figure 2: Synthetic emission line intensity spectra evaluated at 1.1 and 1.3 solar radii. Typical intensities of the K-corona from Münch (1966) were included (the F-corona is negligible at these heights), and thermal emission from an instrument cooled to liquid nitrogen temperatures (a 77K black body spectrum—actually this is so weak that it is not visible on the plot). Line intensities plotted are peak intensities assuming a line width (w=FWHM) of 30 km s^{-1} in Doppler units (thus, the peak intensities shown are approximately integrated intensities divided by the wavelength measured in μm). No other source or sink of IR light is included in this plot (e.g. from thermal emission, scattering or absorption in the Earth's atmosphere). Line identifications are marked for lines whose peak intensities (i.e. in the absence of continuum emission) exceed 20% (arbitrarily) of the neighboring background intensity.
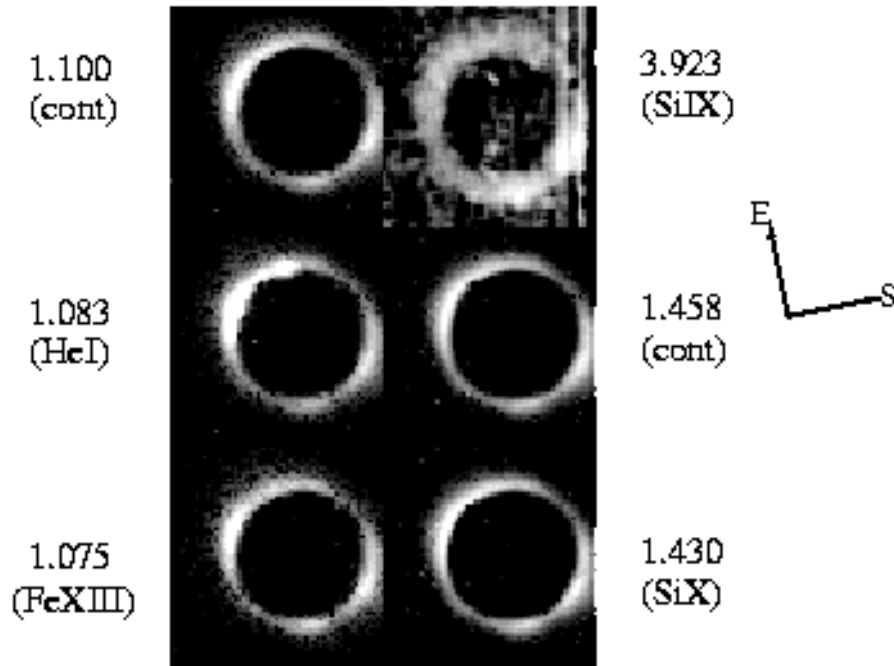
Figure 3: Narrow band filter images at various infrared near wavelengths, from Kuhn et al. (1999).

2.2   Status of forbidden line spectroscopy

Currently, coronagraphic measurements of the E-corona are being made at the following sites[4]:

- Sacramento Peak, New Mexico (data for the Green and Red lines are acquired daily using the Evans coronagraph).

- Norikura, Japan: Red and Green-line imaging system.

- Haleakala, Hawaii.

- Pic du Midi, France.

   To the authors' knowledge, no measurements of emission line polarization are currently being made.

   It has been noted already that the Red and Green line intensity data, formed near 1 and 2 million K respectively, not only sample different regions of the corona, but they differ in physical appearance. Images obtained in the Red line (1MK plasma) generally appear *sharper* than those in the Green line (2MK) (e.g., Bray et al. 1991). This is qualitatively confirmed in high resolution TRACE data, as seen for example in Figure 4.

---

[4]There may be others. The C1 coronagraph of the LASCO instrument on the SOHO spacecraft no longer has this capability.

The cause of this interesting difference is unknown, but it shows that:

> **. . . we should try to develop an instrument capable of measuring emission representative of plasma at both 1 and 2MK. In the remainder of this report we will address some important issues and propose criteria that a new instrument devoted to forbidden line magnetometry should meet.**

2.3   Coronal M1 lines in a physical context

Before proceeding with practical issues, we must complete the discussion of the physics of the formation of the Stokes profiles in M1 lines. The first step is to look at the physical regimes under which the emission lines of the atomic ions form in the Sun's corona. Landi Degl'Innocenti (1983) has given a classification scheme according to the three parameters:

$x = R_a/R_i$: The ratio of anisotropic to isotropic contributions to the radiative excitation rate of the upper atomic level,

$y = \nu_L/\Delta\nu_D$: The ratio of the Larmor frequency $\nu_L = \mu_B|\vec{B}|/h$, (μ_B = the Bohr magneton), to the Doppler width of the line (also in frequency units),

$z = D/R_i$: Ratio of the collisional depopulation rate to the isotropic radiative excitation rate of the upper atomic level.

Landi Degl'Innocenti's classification scheme is illustrated in Figure 5, which (with Figure 6) should be interpreted as follows. The "field strength" regime, determined by parameter y, can be found from Figure 5 panel (a), given a certain magnetic field strength, by examining where the resulting atomic Larmor frequency lies relative to the Dopper width expressed in frequency units ($\Delta\nu_D$) and the inverse lifetime (Einstein A coefficient) of the upper atomic level[5]. The regime of "atomic polarization" induced by anisotropic irradiation, assuming particle collisions are isotropic, can be found in a similar fashion in Figure 5 panel (b), given a value of parameter $x = R_a/R_i$ relative to the collisional depolarization rate parameter $z = D/R_i$.

---

[5]A is the inverse mean lifetime for a simple two level atom. Sometimes, as in Figures 5 and 6, the Einstein coefficient is defined to be $\mathcal{A} = A/2\pi$ so that the lifetime is $(2\pi\mathcal{A})^{-1}$, but in this document A is simply assumed to be the inverse lifetime.
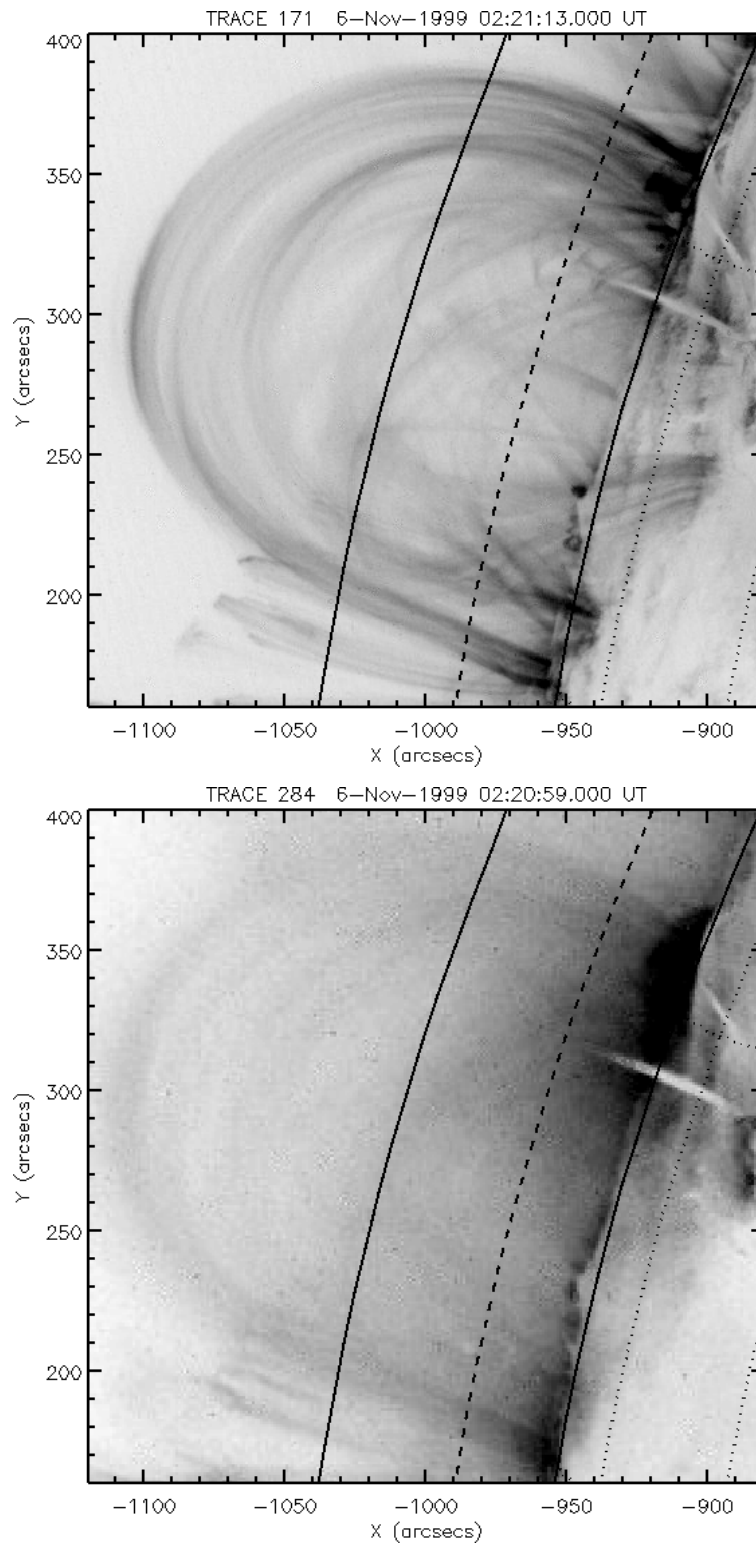
Figure 4: An active region at the limb seen through the 17.1 nm (top panel) and 28.4 nm (lower panel) filters of the TRACE spacecraft, showing post-flare loops (Aschwanden et al. 2000). The 17.1 nm filter responds to plasma predominantly emitting photons from Fe IX and Fe X ions, formed near electron temperatures of 10^6 K, under typical solar conditions. The 28.4 nm filter responds to plasma predominantly emitting photons from Fe XV ions, formed typically near electron temperatures of 3×10^6 K. The solar chromospheric limb is seen at the right edge of the Figure and is marked with a thick line. The position of the edge of occulting disks with radii of 1.05 and 1.10 $R_\odot$ are shown as dashed and solid lines respectively. The instrument's angular resolution is similar in both images.

Figure 5: Polarimetric observations of spectral lines can be classified into fifteen different regimes according to the value of the magnetic field strength (a), (five regimes separated according to magnitude of the Larmor frequency relative to the Doppler and natural linewidths, in frequency units), and according to the relative anisotropy of the incident radiation field and the rate of depolarizing collisions (b) (three regi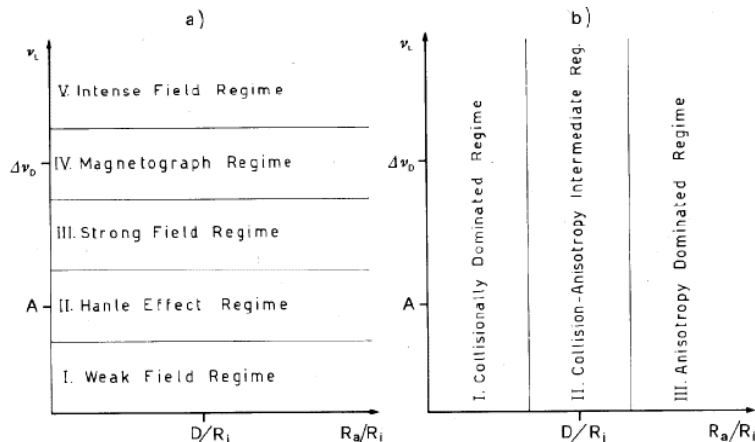mes). The ordinates are proportional to the field strength (which is proportional to the gyro-frequency ν_L), and the abscissae are proportional to the ratio $x = R_a/R_i$ of anisotropic to isotropic irradiation rates. Note that the value of A marked on the ordinate should be multiplied by 2π to be compatible with usual convention adopted in the text.

In the quiet Sun's corona, the magnetic field strength is expected to be $\lesssim 10$ Gauss (Table 1). The coronal plasma is hot, $\sim 10^6$ K, leading to large values of $\Delta\nu_D$. The parameter $y = \nu_L/\Delta\nu_D$ is then much less than unity for all coronal lines. For the particular case of magnetic dipole (M1) transitions between the ground levels of coronal ions, which lie at visible or IR wavelengths, this ratio is 10^{-3} or less. E1 transitions seen at EUV wavelengths by a variety of spacecraft (SOHO, TRACE for example), have values of y which are an order of magnitude or more smaller, because of the larger values of $\Delta\nu_D$.

The anisotropy of the incident radiation at visible and IR wavelengths is always substantial, because the Sun's lower atmosphere (from which such radiation originates) subtends less than 2π steradians as seen from a point in the corona.

Panel (a) of Figure 5 shows us that spectral lines formed in the corona fall into two other regimes, depending additionally on the inverse lifetime (A, units s^{-1}) of the upper level of the transition:

"Hanle effect" regime (Large A or weak field strength such that $2\pi\nu_L \lesssim A$). The magnetic field is strong enough to (partially) relax irradiation-induced coherences between magnetic sublevels. Under solar conditions, this is usually in a regime where the lifetimes of the associated atomic levels are very small, 10^{-7} seconds and less, and therefore applies to radiatively excited electric dipole (E1) transitions, such as the E1 transitions of H I and He I observed at visible and IR wavelengths in prominences (Landi Degl'Innocenti 1982), the Lyman α line (Bommier and Sahal-Bréchot 1982), or perhaps the O VI 1032Å line (Sahal-Bréchot et al. 1986), both seen with the UVCS instrument on SOHO (e.g. Kohl et al. 1998).

"Strong field" regime (Small A or large field strength such that $A \ll 2\pi\nu_L$) The inequality shows that irradiation-induced coherences are negligible (Sahal-Bréchot 1974a, 1974b, 1977). This is an asymptotic regime for the Hanle effect where the scattered linearly polarized radiation has become insensitive to the magnetic field strength, so only information on the orientation of the field vector in the POS is retained.

"Weak field" limit (Weak field strength or large Doppler linewidths such that $\nu_L < \Delta\nu_D$). This inequality, which simply says $y < 1$, states that the field is, in another important sense, relatively "weak" In this case there is a small Zeeman splitting relative to the Doppler widths of the lines, allowing the use of the Taylor expansion of the emission coefficients in terms of the small parameter y to determine the Stokes profiles. The resulting small Stokes V signal, of order yI, can be use to determine the sign and magnitude of the LOS field strength. The Stokes Q, U profiles induced by the transverse Zeeman effect alone in this regime are of order $y^2 I$, they are swamped by the atomic polarization discussed next, and are therefore unlikely to be of practical use for field determinations.

> **There is an unfortunate use of the words "strong" and "weak" in the literature which can lead to confusion. In the absence of considerations of the Hanle effect, the ratio $\nu_L/\Delta\nu_D$ defines the strong ($\gg 1$) or weak ($\ll 1$) field limits. When consideration is given to the Hanle effect, which usually is important at much weaker field strengths than the "weak field" limit, a further parameter, namely $2\pi\nu_L/A$, enters the discussion. In order to avoid possible confusion with the "weak field" limit, House (1977) refers to this "strong field" regime, $A \ll 2\pi\nu_L$, as "effectively strong field". Using this nomenclature, the M1 lines thus fall both in the "strong field regime" and the "weak field" limit!**

Panel (b) of Figure 5 shows the last needed physical parameter needed for complete classification: i.e. the rate at which depolarizing collisions (e.g. with electrons, protons, neutral hydrogen atoms) occur. The regime II(b)[6] in Figure 5 defines the regime where polarization through anisotropic irradiation occurs at a rate comparable to the depolarizing collisional transitions, i.e. $x/z = R_a/D \approx 1$. Landi Degl'Innocenti (1983) estimates that, for E1 transitions formed under typical conditions in the solar atmosphere, this occurs at "critical" particle densities close to 10^{15} cm^{-3}. Thus, for E1 transitions, which to astrophysicists are the most familiar transitions, the regimes I(b), II(b) and III(b) correspond to conditions in the *photosphere, chromosphere and corona* respectively. In contrast, M1 transitions formed in the corona lie in the regimes III(a) (strong field regime) and II(b) ($x/z = R_a/D \approx 1$) for particle densities close to 10^8 cm^{-3}.

In summary, and in the context of other solar observations, Figure 6, from Landi Degl'Innocenti (1983) shows how the M1 lines fit into the whole scheme. Polarization measurements in the corona (including prominence plasma) fall exclusively in the middle- and lower-right portions of the Figure. These are regimes of weak Zeeman-polarization signatures ($y = \nu_L/\Delta\nu_D \ll 1$), and of substantial anisotropic irradiation (significant atomic-polarization signatures), modified by the depolarizing effect of collisions ($D \sim R_a$). Furthermore, the coronal forbidden lines (M1 transitions, marked "Fe XIII, Fe XIV observations in the corona" by Landi Deg'Innocenti), which constitute the bulk of the spectrum of the E-corona, lie in the regime $D \sim R_a$, i.e. collisional depolarization rates and atomic polarization rates induced by anisotropic radiation are of a

---

[6]By using this notation we refer to panel (b), column II in Figure 5.

comparable magnitude. For both lines the Einstein A-coefficients are very much smaller than the Larmor frequency: the transitions find themselves in the "strong-field" regime.
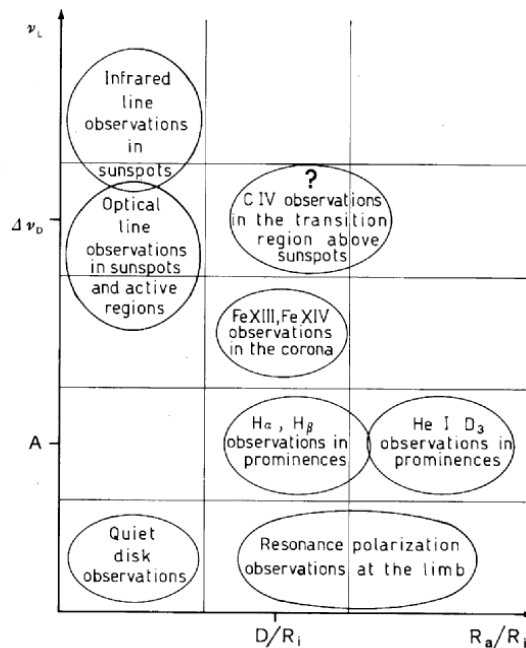

Figure 6: Various solar observations using spectral lines are shown in the classification scheme of Landi Degl'Innocenti (1983). Again, note that the value of A marked on the ordinate should be multiplied by 2π to be compatible with usual convention adopted in the text.

2.4 Overview of the formation of coronal emission line Stokes Profiles

A partial discussion of the details of the formation of coronal M1 lines is given by Casini & Judge (1999, and *erratum* in Casini & Judge 2000). In that paper, the formalism of irreducible spherical tensors was used to illuminate the essential physics by bringing out the basic symmetries in the simplest way (Sahal-Bréchot 1977), and the non-relativistic quantum theory for atom-radiation interactions, developed by Landi Degl'Innocenti and colleagues, was used[7]. The physical regimes outlined above lead to several simplifying assumptions in the spectral formation calculations which have been laid out clearly, e.g., by Sahal-Bréchot (1974a, 1974b, 1977). The most important are:

– The corona is optically thin to all important radiation and is irradiated by spectrally feature-less, unpolarized radiation from the underlying atmosphere.

– The "strong-field" regime is applicable. The ionic density matrix in the atomic eigenfunction representation (the "standard basis"), $\rho(M, M')$, is therefore diagonal in (M, M'), if we take the direction of the magnetic field as the quantization axis. In the irreducible spherical tensor representation, this means that only the coefficients of the density matrix ρ_Q^K with $Q = 0$ are non-zero.

---

[7]This theory is formally equivalent to the more familiar theory based on the expansion of wavefunctions in terms of eigenfunctions of the atomic Hamiltonian, that was used by House (1977).

– All other states (including more highly excited levels which may have natural widths $\sim$ Zeeman splittings) are populated "naturally" (i.e. equal magnetic substate populations). For bound states, this assumption is valid because they lie high enough in energy that photo-excitation is negligible, thus the levels are excited primarily by isotropic particle impact. Transitions involving ionization or recombination can involve initial states whose levels have atomic alignment (for example, recombination from aligned levels in Fe XIV to levels of Fe XIII), but these rates are usually substantially smaller than the bound-bound rates between levels of the same ion. We conclude that coherences (ρ_Q^K, $Q \neq 0$) are negligible and need not be calculated.

– $y \ll 1$ ("weak field" limit).

– Colliding particles have Maxwellian (hence isotropic) distribution functions.

In terms of the density matrix for the radiating ion, we can define atomic *population, orientation,* and *alignment* of a level specified by quantum numbers (αJ) respectively by:

$$\rho_0^0(\alpha J) = \sum_M \rho_{\alpha J}(M, M) \tag{2}$$

$$\rho_0^1(\alpha J) = \frac{\sqrt{3}}{\sqrt{\Pi_J}} \sum_M M \, \rho_{\alpha J}(M, M) \tag{3}$$

$$\rho_0^2(\alpha J) = \frac{\sqrt{5}}{\sqrt{\Pi_J (2J-1)(2J+3)}} \sum_M [3M^2 - J(J+1)] \, \rho_{\alpha J}(M, M) \tag{4}$$

where $\Pi_J = J(J+1)(2J+1)$. These equations give the density matrix coefficients expressed in the irreducible spherical tensor formalism as functions of the (diagonal) density matrix coefficients in the standard basis. In the absence of atomic coherences, the incident radiation, being directed but unpolarized, can generate only *population* and *alignment,* and hence only Stokes I, Q, U. The Zeeman effect generates predominantly Stokes V (the transverse Zeeman-induced linear polarization (Q, U) in the lines, second order in y, is overwhelmed by resonance scattering which has zeroth order terms in y). The Stokes V profiles are dominated by the first order term in y, which in the absence of atomic alignment and orientation leads to the well-known magnetograph formula (as given in elementary texts, e.g. Stix 1989). The radiation-induced additional atomic alignment leads to a systematic modification of this formula.

These conditions lead to the following qualitative picture for the formation and interpretation of forbidden coronal lines. *Linear polarization* measurements rotated to a frame where $Q \neq 0$ and $U = 0$ yield the (projected) direction of the magnetic field in the POS with an ambiguity of $90°$. This ambiguity arises because the magnitude of the linear polarization is proportional to the "alignment factor" $\sigma_0^2(\alpha J) = \rho_0^2(\alpha J)/\rho_0^0(\alpha J)$, which in turn is (approximately) proportional to the "anisotropy factor" of the radiation field, J_0^2/J_0^0, evaluated in the frame of reference of the magnetic field. J_0^2 changes sign as the inclination angle of the magnetic field with the solar vertical, ϑ_B, passes through the Van Vleck angle ($\approx 54°.7$; e.g., House 1977). Thus, because the sign of $\sigma_0^2(\alpha J)$ is in principle not known, an additional ambiguity arises besides the well-known $180°$-ambiguity of all polarization measurements[8]. *Circular polarization* depends on

---

[8]It may be possible to devise a scheme to determine the sign of the alignment factor $\sigma_0^2(\alpha J)$, and hence remove the $90°$ ambiguity, in a manner somewhat analogous to that proposed for permitted lines by Landi Degl'innocenti and Bommier (1993). Such an approach would use the extra information that is encoded in the Stokes I profile (Casini and Judge 1999, equation 35a). Further work is necessary on this point.

$\mathcal{K} = [1 + a\,\sigma_0^2(\alpha J)]/[1 + b\,\sigma_0^2(\alpha J)]$ times the magnetograph formula, where a depends on atomic parameters and b depends also on ϑ_B [Casini and Judge 1999, equation (41)].

In words: Stokes Q and U have contributions from atomic alignment and can yield constraints on the direction of the projection of $\vec{B}$ in the POS; Stokes V is modified by the presence of atomic alignment but the magnetograph formula can yield constraints on the magnitude and direction of the magnetic field along the LOS. In summary then, the polarization of M1 lines contains the following diagnostic information:

- The *magnitude* $P = \sqrt{Q^2 + U^2}$ of the linearly polarized light is sensitive to particle densities n_i and temperatures T_i because collisional depolarizing rates are $D = \sum_i n_i \alpha_i(T_i)$ s^{-1}, with $\alpha_i = \langle v_i \sigma_i \rangle$ cm^{-3} s^{-1} being the collisional depolarization probability per impacting particle of species i, averaged over the velocity distribution function (here assumed to be Maxwellian).

- The *direction* of the linearly polarized light is sensitive to the magnetic field direction (which sets a preferred quantization axis for the atom), and can yield constraints on the direction of the coronal magnetic field, projected onto the plane of the sky.

- The magnitude and sign of the Stokes V profile is sensitive to the LOS magnetic field strength and sign through a variation of the magnetograph formula relating the observed V profile to the frequency derivative of the intensity, I. The generalization is such that the standard formula:

$$V_\nu = -g_{\text{eff}}\,\nu_L \cos\theta_B\,\frac{dI_\nu}{d\nu}\ ,\tag{5}$$

  where g_{eff} is the effective Landé factor of the transition, $\nu_L \propto |\vec{B}|$ is the Larmor frequency, and θ_B is the angle between the magnetic field vector and LOS, becomes

$$V_\nu = -g_{\text{eff}}\,\mathcal{K}\,\nu_L \cos\theta_B\,\frac{dI_\nu}{d\nu},\quad 2/3 \le \mathcal{K} \le 2\ .\tag{6}$$

Equation (6) shows that measurements differential in frequency (or wavelength) are required to interpret the Stokes V_ν profile. In contrast, to interpret Stokes Q_ν and U_ν profiles requires only frequency -integrated data, since they are dominated by terms depending on the zeroth frequency derivative of the emission coefficient. Earlier work based on the resonance polarization effect alone could therefore use quite broad-band filters which did not resolve the line profiles (as done for example on the KELP instrument, Querfeld 1977).

2.5   Measuring magnetic fields using M1 emission lines

Based on the above formation mechanisms for M1 lines, the principles behind measuring properties of the magnetic field are straightforward. They are:

- Select emission lines (e.g. Fe XIII 1.0746 μm, 1.0798 μm).

- Obtain total Stokes parameters (I_λ, Q_λ, U_λ, V_λ) for each selected wavelength λ across the line profile, at each place of interest in the plane of the sky. Perform necessary corrections for scattered light, apply calibrations, and obtain solar Stokes parameters.

- Determine $B_\parallel$ from the first order expansion of the V_λ profile in terms of $dI_\lambda/d\lambda$. With $\nu_L = \mu_B |\vec{B}|/h$, transforming equation (5) to intensity units per unit wavelength, and writing $B_\parallel = |\vec{B}| \cos\theta_B$,

$$V_\lambda = \mu_B \, \bar{g}_{\text{eff}} \, B_\parallel \, \frac{dI_\lambda}{d\lambda} \, \frac{\lambda^2}{10^4 hc} \tag{7}$$

where $\bar{g}_{\text{eff}}$ is the effective Landé factor for the transition, which could also include an estimate of the term $\mathcal{K}$ in equation (6)[9].

- Determine the direction (not magnitude) of the field in the POS from the values of Q and U (integrated over wavelength).

- Examine the magnitudes of the intensity and linear polarization compared with homogeneous models to attempt to determine the influence of depolarizing collisions. If necessary correct the magnetograph formula for the effects of atomic alignment (i.e. set limits on the departure of $\mathcal{K}$ from unity).

2.6 Importance of linear polarization in M1 emission lines

Some of the steps outlined immediately above have already been taken. Observations have revealed that the magnitude of linear polarization is generally less than computed. For example, the Green line was found to be a factor of 3 or so less polarized than computed (Arnaud 1982). The data also reveal (surprisingly, perhaps?) that the dominant direction of polarization is radial- we could speculate that this is related to the low angular resolution of all earlier measurements. But the exact meaning of these results remains unclear. Several different effects can be expected to reduce the observed polarization.

It has been shown that modest density inhomogeneities alone can reduce the large computed linear polarization to bring it into agreement with observations (e.g., Arnaud 1982). This hypothesis can be tested to some degree through observations of *both* forbidden lines of Si-like ions, for example in Fe XIII,

$$3s^2 3p^2 \; {}^3\text{P}_1 \quad \rightarrow \quad 3s^2 3p^2 \; {}^3\text{P}_0 : \quad \lambda = 1.0746 \; \mu\text{m} \; ,$$
$$3s^2 3p^2 \; {}^3\text{P}_2 \quad \rightarrow \quad 3s^2 3p^2 \; {}^3\text{P}_1 : \quad \lambda = 1.0798 \; \mu\text{m} \; ,$$

and the ratio of intensities of the 1.0798 to 1.0746 μm depends not only on radiative excitation of these levels but also quite sensitively on the electron and proton collisional rates (e.g. Penn et al. 1994). Recognizing the inherent problems associated with line ratio diagnostic techniques (Judge et al. 1997), it should nevertheless be possible to set limits on the magnetic field and plasma properties that are compatible with the data.

Measuring such line ratios should be an important additional goal of a coronal magnetometry program, also because other effects, potentially of considerable interest, might also contribute to the discrepancy between observation and theory. For example, the LOS integrals for the emergent Stokes profiles might have changes in the POS-projected magnetic field direction that arise from twisted fields or simple line of sight contributions from different structures. In recent years, a considerable body of work has looked into the kinetics of particles in the corona, driven by the need to understand coronal heating and dynamics, and data both from *in situ* measurements of particle distribution functions beyond the trans-Alfvén point of the flow (e.g. Marsch 1990), and from remotely sensed observations of the corona within a few solar radii of the surface using the UVCS instrument on SOHO (e.g., Kohl et al. 1998). It is

---

[9]Note that for a fixed Doppler linewidth ξ measured in velocity units (equivalently a fixed "ion temperature"), $\frac{dI_\lambda}{d\lambda} \propto \lambda^{-1}$ so that $|\frac{V}{I}|$ scales with wavelength λ as $B_\parallel \cdot \lambda$, confirming the earlier qualitative statement that the longitudinal Zeeman induced V profile scales with increasing wavelength.

possible that kinetic processes might be relevant to the forbidden line polarization problem in
the following sense. Proton collision rates between the levels in the ground terms of ions such as
Fe XIII or Fe XIV tend to increase with increasing proton temperature T_p (e.g. Landman 1975),
but the corresponding electron collision rates decrease with increasing electron temperature T_e.
Thus, polarization observations might be used to limit T_p/T_e. This could be of considerable
interest in theories of coronal heating (e.g. Marsch and Tu 1997). Forbidden line data would
preferentially sample closed field regions, unlike the UVCS measurements that have sampled
(primarily) open field regions.

Depolarizing collisions must be considered individually for each line of interest, and such
work is in progress (Judge and Casini 2001). Some idea of the effects can be estimated from the
work of Judge (1998; specifically the lower panel of his Figure 1), who studied only inelastic and
super-elastic collisions. Specific lines (e.g., Fe XIII 1.0746 μm) have significant contributions to
the intensity from radiative excitation for all heights in the corona, and can be expected to be
influenced by atomic alignment. Other lines (e.g., Si IX 3.9346 μ) having large contributions
from collisions low in the corona (below $\sim 0.4\,R_\odot$) are expected to be less affected by atomic
alignment, at least at low heights.

> **Measurements of magnetically *and* density sensitive lines (e.g. the
> 1.0746 vs. 1.0798 μm lines of Fe XIII) will help to determine the
> cause of the known discrepancy between observed and computed
> linear polarization of M1 lines. Resolution of the discrepancy po-
> tentially has consequences for the identification of current systems,
> and might even set interesting limits on the ratio of proton to elec-
> tron temperatures in the corona.**

2.7   Limitations and practical considerations

The preceding discussion reveals the following important *fundamental limitations* to diagnostic
techniques based upon M1 emission lines:

- The vector field is not directly constrained by observations: the magnitude of the vector field
  is constrained by the Stokes V profile through use of equation (6), but only along the LOS.
  In the POS, the field strength may be any reasonable value, only the direction projected
  onto the POS is constrained by Stokes Q and U. This has a $90°$ ambiguity (although see the
  footnote on page 21).

- Data obtained from one vantage point (e.g., the Earth) are spatially of a two-dimensional
  nature (I, Q, U and V are measured only in the POS), but the field is obviously three dimen-
  sional. Thus, additional information is needed to try to reconstruct a picture of the three
  dimensional field from its LOS integrated signature. Stereoscopic observations, even of the
  solar photosphere, are not yet available.

- The LOS integrals that lead to the observed I, Q, U, V profiles have important *null spaces*,
  i.e. there exist configurations of plasma and magnetic fields for which the magnetic fields are

non-zero but which, when summed along the LOS, do not contribute to the emergent Stokes parameters. One simple example is if the three dimensional thermal and magnetic structure is exactly symmetric upon reflection through the POS: the Stokes V profile is exactly zero in this case.

There is a potentially important *simplification* in the interpretation of coronal M1 lines compared with photospheric lines: the "filling factor" of the magnetic field is unity in a low-β plasma. If the plasma is all in a low-β state, there is no need to determine the relationship between flux density per unit area and magnetic flux density- they are essentially equal. An important exception of interest might be current sheets in, for example, "x-type" neutral sheets, where the field strength is zero along the sheet but the plasma pressure is higher (to offset the imbalance in the neighboring magnetic stresses).

Because of these limitations, one must augment the data with *physical models*, and with *other observations*. Simple physical constraints such as div $\vec{B} = 0$ might be used with measurements of photospheric fields, prominence fields (where associated with the coronal data of interest) and morphology of E-coronal Stokes images, for example, to determine likely magnetic configurations along the LOS.

> **Coronameter data of M1 lines are *fundamentally limited in their ability to determine vector magnetic fields throughout the corona*, because of (1) line of sight integration problems, and (2) the limited information contained on $\vec{B}$ (POS direction, LOS sign and strength). Therefore M1 emission line data should be analyzed in conjunction with other measurements, including prominence data, wherever possible. A synoptic program would in principle allow analyses with synoptic photospheric magnetic field data, and tomographic techniques.**

There remain additional issues that require attention, which we will discuss in order, from atomic, solar, atmospheric to instrumental:

- Which lines of which ions should we try to observe in order to (a) shed most light on the "inverse problem" in general, (b) shed most light on the different characteristic features observed in the Sun's corona (quiet Sun, active regions, streamers, coronal holes, prominences, CME's)?

- What issues remain with regard to the influence of the Earth's atmosphere? Emission, scattering, absorption, time variations are all critical issues to be understood. These will determine for instance, whether a mountain site suffices or whether one must go to a space-based platform to do the job right.

- Are there important issues concerning telescope optics, polarimeter design, and detector(s), that will influence the choice of spectral lines?

- Are there issues that cannot be answered with presently available data, i.e. do we need to acquire more atomic, atmospheric or other data to answer the above questions?

Our task henceforth is to try to see if we can determine a design/platform of an instrument to optimize the scientific return, of course at reasonable cost.

3 Selection of Lines

3.1 A first cut

Relatively few ions are abundant in the quiet Sun's corona, and (aside from protons, α particles, and ions of the H and He isoelectronic sequences which have no useful magnetically sensitive spectral lines) these all belong to elements from the third and fourth row of the periodic Table. Correspondingly, there are relatively few M1 transitions likely to be strong enough and otherwise suitable for polarization measurements of the Sun's coronal magnetic field. Based upon atomic structure and abundance and thermodynamic considerations, Judge (1998) has searched for all possible transitions (not limited to M1 transitions, but all optical and infrared transitions in abundant ions). Table 4, based upon Judge's (1998) Table 3, includes some simple estimates of the background noise and lists prominent absorbers in the earth's atmosphere from calculations discussed below. It includes lines of ions that are of the most interest.

The data in the Table were derived from specific intensities, integrated over wavelength and solid angle, to give total photon flux densities from the entire corona as seen from the earth. For lines, the flux densities are integrated over the line profile. For continua, the flux densities apply to the wavelength integrations over the full width at half maximum of the lines[10].

Table 4: Characteristic properties of candidate M1 lines

Ion	λ μm	$\tilde{\nu}$ cm^{-1}	Log $T_{\rm e}$ K	$F_{\rm E}$	$F_{\rm scat}$ ph cm^{-2} s^{-1}	$F_{\rm th}$	Absorber	Transm. % 8km
Fe XIV	0.530	1.885+4	6.30	2.57+8	2.78+8	8.22-32	...	100
Fe X	0.637	1.568+4	6.03	1.77+8	1.37+8	3.96-24	...	100
Fe XI	0.789	1.267+4	6.10	1.48+8	5.48+7	7.21-17	...	100
Fe XIII	1.075	9.305+3	6.22	4.91+8	1.26+7	7.27-9	...	100
Si X	1.430	6.993+3	6.13	1.57+8	2.88+6	1.85-3	H_2O +0.2cm^{-1}	50
S XI	1.920	5.208+3	6.25	3.59+7	5.85+5	2.21+1	H_2O	50
Si IX	2.584	3.870+3	6.04	6.07+7	1.11+5	2.01+4	H_2O	0
Fe IX	2.855	3.503+3	5.94	1.60+7	6.31+4	1.23+5	$H_2O/CO_2/N_2O$	60
Mg VIII	3.027	3.303+3	5.92	2.73+7	4.51+4	3.27+5	(H_2O+0.6cm^{-1})	100
Si IX	3.935	2.545+3	6.04	5.67+7	1.01+4	1.17+7	N_2O	60
Mg VII	5.502	1.818+3	5.80	3.20+6	1.42+3	2.80+8	H_2O	10
Fe XI	6.081	1.644+3	6.10	2.61+6	7.88+2	5.62+8	H_2O	50
Mg VII	9.031	1.107+3	5.80	9.53+5	7.66+1	3.79+9	O_3	90

λ, $\tilde{\nu}$: wavelength, wavenumber of the transition; Log $T_{\rm e}$: $T_{\rm e}$ is the electron temperature at which the ion's population is a maximum; $F_{\rm E}$: unattenuated photon flux densities from the entire corona, as seen by a perfect coronagraph that just masks the chromosphere; $F_{\rm scat}$: photon flux densities over the bandwidth of the emission line that is scattered from the Earth's atmosphere, calculated using conditions of a good coronal site (2×10^{-5} of the disk brightness at 0.5 μm), varying with λ^{-4} (Rayleigh scattering from molecules). Scattering from small particles (aerosols) varying much less steeply ($\propto \lambda^{-\alpha}$ with $0 < \alpha < 4$), is not included; $F_{\rm th}$: upper limits to thermal emission over the same bandwidth, calculated from a $2R_\odot$ radius disk radiating a Planck function at 250K; Principal telluric absorbers over the bandwidth of the observed line, and the extinction features (in percent), calculated for the Sun at zenith from an altitude of 8km. Emission from the K-corona is not listed: it is $\sim 10^{-6}$ of the disk brightness, which translates to $1 \times 10^7 \lambda$ in units of ph cm^{-2} s^{-1}.

The entries in Table 4 reveal some important trends:

---

[10]These calculations were made for a proposed aircraft experiment flying at 8 km that was scrapped in 1998. Nevertheless the numbers in the Table are of interest to the present report.

1. Strong lines are present from visible wavelengths to about 10 μm, spanning electron temperatures from 5.8 to 6.3 in logarithmic units (degrees K).

2. The unattenuated line flux densities decrease almost monotonically with increasing wavelength because of simple trends in atomic properties[11].

3. The background or "noise" terms F_{sc} and F_{th}, arising from scattering and thermal emission in the Earth's atmosphere, have radically different dependencies on wavelength. F_{sc} is a rapidly decreasing (power-law) function of wavelength, F_{th} is an exponentially increasing function of wavelength.

4. The dominant source of absorption opacity at the wavelengths of the lines is *water vapor*. Some of the detrimental effects of the earth's atmosphere therefore can be minimized by observing from a high, dry mountain site.

> **No other coronal ions than those listed in Table 4 need be considered for a magnetometer, although some other lines of the listed ions will be useful.**

3.2   Flux budget: ideal conditions

To make more accurate estimates of photon fluxes, we have adopted the "representative" coronal model of Judge (1998), with reasonable instrumental properties, and have used the simple magnetograph formula which is accurate to a factor of 2 (ignoring the null-space problem noted in Section 2.7). Details of the specific calculations made are listed in Table 5. Numbers are given for the 1.0746 μm line of Fe XIII which, as we will see, is one of the most promising lines for magnetometer work. We will first estimate a photon flux budget, for an instrument that is free from the influence of the earth's atmosphere and which has no sources of light other than from the E corona. There is no specific design here, but we have in mind a coronagraph that will image the solar corona onto a spectrograph slit, with polarization optics inserted at an appropriate place in the optical path, which then images the measurable combinations of Stokes profiles (e.g. $I + V$) onto a detector array. The overall efficiency of the entire system is simply replaced by 10% (i.e. only 10% of those photons impinging on the telescope objective register as counts on the detector).

   Using the data in Table 5, we can estimate the number of photon counts per pixel on a detector placed at the focal plane of the system, as follows. First, we assume that the corona

---

[11]These trends can be understood simply in terms of the charge on the ion in which the optical electron moves, at least for highly charged ions where the strong Coulomb force from the nucleus dominates the Hamiltonian. For a given M1 transition in a given isoelectronic sequence, wavelengths tend to decrease sharply with increasing ionic charge Z. In turn, radiative transition probabilities increase sharply with increasing Z, but collision rates decrease. These atomic properties are summarized, for example, by Dufton and Kingston (1981). But additionally, the intensity of the photospheric radiation decreases with increasing wavelength in the Rayleigh-Jeans limit. Thus, both photo-excitation rates and the probability of photon escape decrease, thereby reducing the intensity of a given M1 transition as its wavelength increases with the decreasing charge along the appropriate isoelectronic sequence.

Table 5: Simulation parameters for Stokes I, V profiles

Physical quantity	Value	Source & Notes
ASSUMED SOLAR QUANTITIES...		
$I_{1.0746}(r = 1.1R_\odot)$	20 $\mathrm{ergs\,cm^{-2}\,sr^{-1}\,s^{-1}}$	Judge (1998), Intensity of Fe XIII line
$I_{1.0746}^{\mathrm{ph}}(r = 1.1R_\odot)$	1.1×10^{12} ph $\mathrm{cm^{-2}\,s^{-1}\,sr^{-1}}$	
ξ	20 $\mathrm{km\,s^{-1}}$	Doppler width
$-\left(\frac{d\,ln\,I_{1.0746}}{dr}\right)^{-1}\|_{r=1.1R_\odot}$	0.08 $R_\odot$	Judge (1998), radial scale height[a]
$B_\|$	10 Gauss	extrapolated
I_K	$10^{-6}B_\lambda(T = 5900)$	Golub and Pasachoff (1997), K-corona Intensity
ASSUMED EARTH ATMOSPHERIC QUANTITIES...		
Atmosphere	Tropical: Mauna Loa	
Line list		HITRAN 1992 Rothman (1992)
Spectral transmittance	0 to 1	GENLN2 Edwards (1992)
I_{aero}	$3 \cdot 10^{-6}B_\lambda(T = 5900)$	Beckers (1995), aerosol scattering
I_{Rayleigh}	$2 \cdot 10^{-5}B_\lambda(T = 5900)\left(\frac{0.5}{\lambda}\right)^4$	Golub and Pasachoff (1997)
ASSUMED INSTRUMENTAL QUANTITIES...		
Station	Mauna Loa	
Altitude	3.397 km	
Objective	$D = 40$ cm, A=1257 cm^2	(= size of Evans objective)
Effective area	125.7 cm^2	(Net efficiency $E = E_{opt}E_{det} = 10\%$)
Angular size of 1 pixel at spectrograph slit	10 arcsec	The 256 spatial pixels cover an area of $0.01R_\odot \times 1.3R_\odot$
Dark current	$\equiv 0.1B_\lambda(T = 300K)$	thermal emission only
Spect. dispersion d_λ	$0.14 \cdot \lambda$ Å/pixel	$N_\lambda = 7$, see text
Integration time t	10^3 sec	for each $I + V$, $I - V$
I_{tel}	$10^{-5}B_\lambda(T = 5900)$	Telescope scattering (diffraction+roughness)

a. This is a factor of two or so smaller than an observation by Kuhn et al. (1996).

is imaged onto the spectrograph slit and that the dispersed image of the slit is further imaged onto a 2D array of (say 256) wavelength by (say 256) spatial pixels. Each pixel collects photons from a 10×10 arcsec^2 solid angle ($\omega \equiv 2.3 \times 10^{-9}$ steradians) of the corona. The flux density of (unpolarized) photons from a 10 arcsec^2 solid angle that enters the telescope (assuming zero losses) is $I_{1.0746}^{\mathrm{ph}} \cdot \omega$ photons cm^{-2} s^{-1}. With a net optical efficiency E_{opt}, and a total objective area A, then the total number of photons incident on the detector (integrated over all wavelengths) is $I^{\mathrm{ph}} \cdot \omega \cdot A \cdot E_{opt}$ photons/sec. Solar M1 line profiles typically spread the line photons over $w = $ FWHM $\approx 10^{-4}\lambda$ μm (e.g., Billings 1965, Tsubaki 1975). If the dispersion d_λ (note: this is in Å px^{-1}) of the spectrograph is chosen such that the number of wavelength pixels covered by the line N_λ is constant with wavelength then d_λ is fixed so that $d_\lambda \approx \lambda/N_\lambda$. For $N_\lambda = 7$ say, $d_\lambda = 0.14\lambda$, as given in Table 5. The typical number of photons incident on each pixel in the detector is then $I^{\mathrm{ph}} \cdot \omega \cdot A \cdot E_{opt}/N_\lambda$ photons sec^{-1} pix^{-1}. If the efficiency of the detector is E_{det} counts photon^{-1}, then, with the effective area of the instrument written as $A_{eff} = A \cdot E_{opt}E_{det}$,

we have $c_I = I^{\mathrm{ph}} \cdot \omega \cdot A_{eff}/N_\lambda$ counts sec^{-1} per spectral pixel. For an exposure time of t sec, the Stokes I profile will then have typically a total of

$$C_I = I^{\mathrm{ph}} \cdot \omega \cdot A_{eff} \cdot t \, / \, N_\lambda \tag{8}$$

counts per spectral pixel. With the values of parameters listed in Table 5, this yields 4.5×10^7 counts pix^{-1}, or 3.1×10^8 counts integrated over the entire line.

The above applies to a measurement of the Stokes I parameter. To determine the Stokes Q, U and V parameters, each requires two measurements (e.g., of $I+V$ and $I-V$). Thus, for the $(I+V)$ measurement for example, since we know that $|V| \ll |I|$,

$$
\begin{aligned}
C_{I+V} &= (I+V)^{\mathrm{ph}} \cdot \omega \cdot A_{eff} \cdot t/N_\lambda \tag{9} \\
&\simeq C_I \, . \tag{10}
\end{aligned}
$$

The r.m.s. uncertainty in the counts for, e.g., $I+V$ from photon counting statistical fluctuations alone is then simply

$$\sigma_{I+V} \simeq \sqrt{C_I} \, . \tag{11}$$

The uncertainties in V must be evaluated from error propagation rules for the measurements of the two quantities $(I+V)$ and $(I-V)$, since $V = \frac{1}{2}(I+V) - \frac{1}{2}(I-V)$. Assuming the error covariance between the two measured quantities is zero, we see that

$$
\begin{aligned}
\sigma_V^2 &= \frac{1}{4}\sigma_{I+V}^2 + \frac{1}{4}\sigma_{I-V}^2 \tag{12} \\
&= \frac{1}{4}C_{I+V} + \frac{1}{4}C_{I-V} \tag{13} \\
&\simeq \frac{1}{2}C_I \, . \tag{14}
\end{aligned}
$$

For $B_\parallel = 10$ Gauss, $g_{eff} = 1.5$, $\mathcal{K} = 1$ and for a line at 1 μm, we expect $|V| \sim 10^{-3}|I|$. So writing schematically $\max(|V|) = \epsilon_V|I|$ where the parameter $\epsilon_V \ll 1$ (the same can be written for the Stokes Q, U parameters and the corresponding parameters ϵ_Q and ϵ_U), we can estimate the peak signal to noise ratio for V, for *photon counting noise only*, as:

$$
\begin{aligned}
\frac{V}{\sigma_V} &\simeq \frac{\epsilon_V C_I}{\sqrt{C_I/2}} \tag{15} \\
&\simeq \epsilon_V \cdot \sqrt{2C_I} \, . \tag{16}
\end{aligned}
$$

Thus, If $\epsilon_V = 10^{-3}$, then a signal to noise ratio of $\frac{V}{\sigma_V} = 3$ would require 4.5×10^6 counts. **This can be achieved with an integration time (for each of the $I+V$ and $I-V$ measurements) of ~ 100 seconds.**

The expected values of $\epsilon_{Q,U}$, originating from the resonance polarization process, are ~ 0.01 to 0.1. Thus, **to get a 3σ signal to noise ratio in Q or U requires just 1 to 0.01 seconds per measurement.** Furthermore, in this case we can take $N_\lambda = 1$ since we require no measurements that are differential in wavelength, decreasing the exposure times by a factor of $N_\lambda \sim 7$ or so, yielding 0.14 to 1.4×10^{-3} s respectively. **This calculation illustrates the extreme difficulty of the longitudinal Zeeman (Stokes V) measurements over and**

above the resonance polarization measurements (Stokes Q and U).   We can see partly why Harvey (1969) made his comments quoted at the end of Section 1.1.

We can summarize these calculations simply as follows. Let the Stokes profiles be I_α, $\alpha = 0\ldots3$, where $I_0 \equiv I$, $I_1 \equiv Q$, $I_2 \equiv U$, $I_3 \equiv V$, then we can write the signal to noise of I_α as

$$\frac{I_\alpha}{\sigma_\alpha} \simeq \epsilon_\alpha \sqrt{2 C_{I_{\alpha=0}}} \tag{17}$$

$$\simeq \epsilon_\alpha \sqrt{2 I^{\mathrm{ph}} \cdot \omega \cdot A_{eff} \cdot t / N_\lambda} \tag{18}$$

where ϵ_α and N_λ are given in Table 6.

Table 6: S/N and exposure time scalings for Fe XIII 1.0746 μm

Stokes parameter	I	Q, U	V
α	0	1,2	3
ϵ_α	$1/\sqrt{2}^a$	$0.01 \rightarrow 0.1$	$\sim 10^{-4} B_\parallel \lambda$
N_λ	1	1	7
s/n given parameters in Table 5	1.8×10^4	$250 \rightarrow 2500$	9.5
Integration time [seconds] to achieve s/n=3 for each of $I_0 + I_\alpha$, $I_0 - I_\alpha$	2.8×10^{-5}	0.0014-0.14	100

a. This is not unity simply because we use eq. (17) which includes the two measurements $I_0 + I_\alpha$, $I_0 - I_\alpha$, but for $\alpha = 0$ obviously only one measurement is needed.

The values of s/n and integration times are given in Table 6 for wavelength-integrated quantities for the Stokes I, Q and U profiles, and for a "typical" value of the wavelength dependent Stokes V profile (given by $\epsilon_3 \cdot \int I_\lambda d\lambda / w$, where w is the full width at half maximum intensity of the Stokes I profile).

Lastly, based on equation (18), we can write down a scaling for the dependence of the total exposure times for the 3σ Stokes V profile, on the various parameters:

For a signal-to-noise ratio of snr in Stokes V, including photon counting noise and the time needed to measure both $I + V$ and $I - V$,

$$t \sim 200\,\mathrm{s} \left(\frac{snr}{3} \frac{10}{px} \frac{40}{D} \frac{10}{B_\parallel} \frac{1.5}{g_{eff}} \right)^2 \frac{1}{\lambda^3} \frac{20}{I_\lambda} \frac{10}{E} \frac{N_\lambda}{7} \tag{19}$$

Where px are measured in arcsec, D in cm, $B_\parallel$ in Gauss, λ in μm, I_λ in erg cm^{-2} s^{-1} sr^{-1}, total efficiency E in %, and N_λ is unitless. *Modest equipment can in principle make useful measurements in reasonable exposure times.*

$E = E_{opt} E_{det}$ is the total efficiency of the system, expressed in equation (19) as a percentage. Photon fluxes are high enough for meaningful measurements of the Stokes profiles to be made in

reasonable exposure times, at least in principle. Below we will include the effects of background emission, scattering and transmission in the telescope and atmosphere. But first we look briefly at uncertainties in the inferred strength and direction of the magnetic field.

> **The above calculations refer to the 1.0746 μm line of Fe XIII. It is interesting to consider the effects of measurement uncertainties in the Stokes V parameters at different wavelengths. For the Si IX line at 3.9346 μm the required exposure time is a only 0.6 times as long (from equation 19 and the relative line intensities listed below in Table 8). In contrast the Green, Red and Fe XI 0.789 μm lines require exposure times that are a factor of 5-10 longer, re-emphasizing the potential power of infrared observations.**

3.3   Limitations imposed by detector characteristics

So far, photon counting noise is the only source of noise considered. Of course, a real camera system will introduce significant new sources of noise through read noise, and pixel-to-pixel gain fluctuations. Consider first the read noise.

Modern InSb detectors have well depths of $\approx 10^6$ electrons, and a read noise ≈ 150 electrons. From the above calculations, in a 10^3 s accumulation time, $C_I \approx C_{I+V} \approx 3 \times 10^7$ counts. To fill the detector wells to the 30% level requires breaking up the accumulation time into 100 separate readouts of 10 s each. Each pixel has a read noise of 150 electrons, a photon counting noise of $\sqrt{300,000} \approx 548$ electrons, a total noise of 568 electrons and a signal-to-noise ratio of 528:1. In the absence of errors introduced through gain corrections, this ratio in the average created by summing the 100 separate readouts is 5280:1. Note that, because the photon counting noise exceeds the read noise, this value is below but still quite close to the "idealized" value of $\sqrt{3 \times 10^7} : 1 = 5477$:1 arrived at using only equation (11).

The effects of detector gain variations cannot be estimated in such a simple way– these must be examined on the basis of measured temporal and spatial variations of detector pixel sensitivity using appropriate flat field exposures. If the detector proves to be quite stable, we can expect gain tables to be accurate to levels better than the noise levels estimated above. We note that, by "dithering" (i.e. deliberately moving the dispersed solar images on the detector) at least some residual gain variations can be reduced significantly.

3.4   Uncertainties in the magnetic field direction and $B_\parallel$

We can estimate the uncertainty in the magnetic field direction in the POS (given by some angle ϕ specified by defining an axis in the POS), and field strength along the LOS, from photon statistics alone[12]. Owing to the non-linear dependence of the linear polarization on the magnetic field orientation, this is difficult, but we may set lower limits to this simply from the photon limited uncertainties in Q and U. Schematically,

---

[12]Again, no account is taken here of the null space problem mentioned in Section 2.7.

$$\frac{\sigma(\phi)}{\phi} \gtrsim \text{sum of errors in } (Q, U) \tag{20}$$

which involves propagation of errors through $arctan$ and ratio functions. This is expected to be of order

$$\frac{\sigma(\phi)}{\phi} \gtrsim \sqrt{[\frac{\sigma(Q)}{Q}]^2 + [\frac{\sigma(U)}{U}]^2} \tag{21}$$

$$\frac{\sigma(\phi)}{\phi} \gtrsim \sqrt{2[\frac{\sigma(Q)}{Q}]^2} \tag{22}$$

$$\tag{23}$$

Given the above results, we in principle can obtain rather precise measurements of ϕ from relatively short integration times.

The uncertainty in $|B_\parallel|$ from photon statistics alone is:

$$\sigma(B_\parallel) = \text{sum of errors in } (\frac{dI}{d\lambda}, V) \tag{24}$$

or

$$\frac{\sigma(B_\parallel)}{B_\parallel} \sim \sqrt{(\frac{\sigma(I)}{I})^2 + (\frac{\sigma(V)}{V})^2} \tag{25}$$

which is to a good approximation (because $\frac{\sigma(V)}{|V|} \gg \frac{\sigma(I)}{I}$) simply

$$\frac{\sigma(B_\parallel)}{B_\parallel} \sim \frac{\sigma(V)}{|V|} \tag{26}$$

We stress these error estimates are lower limits, being from photon counting statistics alone, with no noise introduced from detectors or from influences of the Earth's atmosphere. It is clear that the polarizer system will have to make measurements of the V profile with a sensitivity of roughly

$$\max \sigma(\frac{V}{I}) = 10^{-4} \frac{B}{[\text{G}]} \frac{\lambda}{[\ \mu\text{m}]} \ . \tag{27}$$

Thus, for mean field strengths of say 10 Gauss, the cross talk from Q,U,I to V, and other sources of systematic error, must be less than 0.0003 times the wavelength in μm, for a "3-sigma" detection.

3.5   Constraints set by influences of the Earth's atmosphere.

The Earth's atmosphere influences polarization measurements in several ways:

- Scattering of light from the solar disk is important. The dominant sources of atmospheric scattered light are:

  * Rayleigh scattering from abundant molecules, important at visible wavelengths. As already noted, for a good coronal site, this is $2 \times 10^{-5} B_\odot \frac{\lambda}{0.5}^{-4}$, for λ measured in μm.

∗ Scattering from aerosols (small airborne particles). This depends on several poorly known quantities, including the size, shape, refractive properties of the individual particles and on their large scale distribution. The larger the size relative to the wavelength, the weaker the dependence on wavelength. For practical purposes the measured number density of particles of size 0.5 μm or larger, that can contribute to the scattering at wavelengths beyond 1 micron, is very small (Smartt and Koutchmy 1995). Beckers (1995) estimates (in his Table 3) that scattering from aerosols contributes ≈ 3 millionths of the solar disk intensity, at $1.15 R_\odot$, dropping to 1 millionth at $2 R_\odot$.

- Unwanted scattered light is generally *linearly polarized*, a situation that complicates the measurement of the Q and U and, through cross-talk, V Stokes profiles of M1 coronal lines. For example, small-angle scattering from aerosols and molecules along the LOS is weakly polarized. Sunlight scattered from the earth's surface and back into the LOS (a double scattering) is highly polarized in a direction parallel to the earth's horizon- its removal is a significant issue in the calibration of HAO's Mk IV white light coronagraph, for example (D. Elmore, private communication 2000). Again, observing at infrared wavelengths with smaller scattering cross sections offers improved conditions for the accurate measurement of solar polarization.

- At visible and near-IR wavelengths, atmospheric *seeing* may be a problem. Occulting disks occult different areas of the solar atmosphere depending on the seeing, but this problem diminishes with increasing observing wavelength. For example, Fried's seeing parameter (usually denoted R_0), measures the transverse distance by which two parallel rays of light must be separated so that the r.m.s. phase delay difference between them (imposed by variations in the atmospheric refractive index) should be some fraction of a wavelength, usually $\lambda/2$. Roughly speaking, it is the size of the largest optically perfect telescope that will make diffraction-limited images through the given atmosphere at the chosen wavelength. R_0 varies roughly as

$$R_0 \propto \lambda^\beta, \quad \beta \geq 1.2, \tag{28}$$

(e.g. Smartt and Koutchmy 1995). There is thus a substantial benefit to making observations at infrared instead of visible wavelengths.

- At wavelengths beyond 1.1 μm, we cannot ignore telluric absorption, predominantly by tropospheric water vapor.

- Beyond roughly 3 μm, we cannot ignore telluric thermal *emission*, mostly from tropospheric water vapor.

- Near 9 μm, mesospheric ozone is a major absorber. For lines at this wavelength, a space-based platform would be advisable, but the weak intensity of lines this far into the infrared discounts them as primary targets for magnetometer measurements.

In an ideal world, all but the last of these influences would present little problem since one could in principle integrate long enough to be able to extract these effects from the raw data to provide Stokes profiles. In practice, these effects are vital to understand and take care of, for several reasons. First, we have seen above that the intrinsic polarization degree P of the emitted coronal light ($P = \sqrt{Q^2 + U^2 + V^2}/I$) is relatively small, 0.1 or less for the resonance polarization signature, and dominated by parameters Q and U. V is much smaller for the longitudinal Zeeman effect, on the order of 10^{-3}. Therefore just a small fraction of the flux

of photons incident on a detector actually contains information on the magnetic field. Second, the Earth's atmosphere is intrinsically variable. The flux of photons on the detector contains not only signal from the solar emission line, but in principle *variable* absorption, emission and scattering from molecules and particles in the atmosphere, especially the troposphere.

To investigate telluric absorption and scattering we performed high spectral resolution transfer calculations using the GENLN2 line-by-line atmospheric transmittance and radiative model (Edwards 1992). The model assumes a multi layered atmosphere of mixed gases and takes into account both spectral line and continuum transitions. Figs. 8 through 15 show, in the second panel from the top of each panel, the atmospheric transmission computed from this model, for conditions representative of the tropics at Mauna Loa Observatory in Hawaii.

These calculations show that the polarimetry must be performed carefully. The atmospheric (absorption) opacity consists mostly of bands of tropospheric water vapor, which have a very strong wavelength dependence. These telluric features will almost certainly be unresolved by any (medium dispersion) spectrograph devised to determine the Stokes parameters of coronal emission lines. The unresolved, time-variable nature of the expected absorption features dictate that one must measure $(I + V)$ and $(I - V)$ simultaneously.

Putting the telluric influences together, we conclude that

> **... although telluric absorption is not strong enough to demand a space-based platform, (with the possible exception of Mg VIII at 3.027 μm), the variable and spectrally unresolved telluric influences force one to measure $(I + S)$ and $(I - S)$ simultaneously, where S is one of Q, U, V, both in the "line" emission core and in the neighboring "continuum". The alternative − to run the system faster than scintillation − would lead to excessive detector read noise.**

3.6   Additional constraints set by the Sun.

Typical thermal conditions in quiet Sun, streamer, active region loops and prominence cavity structures indicate that we should measure Stokes profiles in lines of ions whose abundance peaks between 6 and 6.5 in log T_e. Most of the ions listed in Table 4 were selected to satisfy this requirement.

The structures seen in the corona in lines of different ionization stages can be noticeably different, as shown, for example, by the synoptic data in Figure 7, by the EUV data acquired by the TRACE spacecraft (Figure 4) and the YOHKOH soft X-ray telescope. It has been recognized for some time that structures seen in the Red line differ qualitatively from the Green line. In fact the terms "Green line group" or "Red line group" have been used to highlight differences between the appearance of loop structures seen at Log $T_e \approx 6.0$ and Log $T_e \approx 6.3$ (e.g. Bray et al. 1991). While this grouping might be considered somewhat arbitrary in physical terms, (for example, while TRACE data such as those shown in Figure 4 suggest that the loops are more sharply defined in the Red than Green line because of real differences in solar thermal conditions, seeing/scattering differences in ground-based observations can also contribute to the effect), it emphasizes the fact that *any proposed coronal magnetometer should have the capability*

to observe lines from both groups. We expect that observations of lines sampling a variety of temperatures will be vital to develop a complete and (hopefully) unique interpretation of the polarization measurements in terms of the underlying magnetic structure.
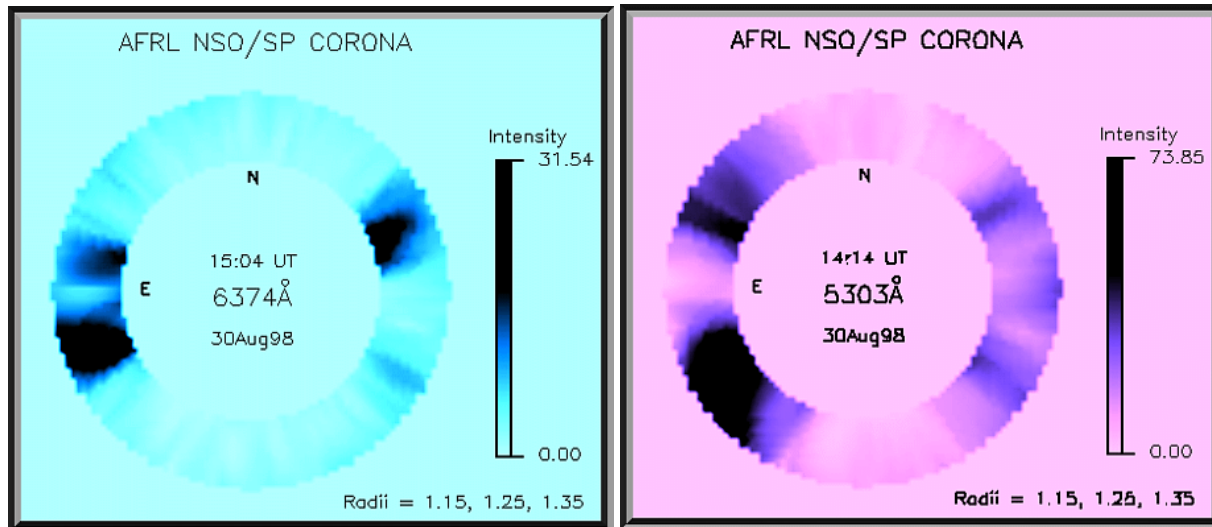

Figure 7: Synoptic data from the Sacramento Peak Evans coronagraph for Fe X, the "Red line", formed at roughly 10^6 K (left), and the Green line of Fe XIV, formed at roughly 2×10^6 K (right). Notice that the spatial structure in these two intensity maps is quite different, even at the relatively coarse angular resolution of these data. Data obtained at higher resolution and at other wavelengths (cf. Figure 4) have consistently revealed additional differences between the Red and Green line groups of lines.

Last, but not least, the solar corona is dynamic, even in quiet regions. For example, in a detailed study of M1 profiles observed with the Sacramento Peak Evans coronagraph at visible wavelengths, Tsubaki (1975) found non-thermal "turbulent" motions of r.m.s. amplitude between 6 and 16 km s^{-1}, with systematic motions of typically 5 but extending up to 12 km s^{-1}. The latter are a significant fraction of the linewidth, meaning that, if not properly accounted for, they would lead to a systematically erroneous application of the magnetograph formula. These observations were reduced using a coarse "binsize" of 5 Mm or 7 arcsec. To properly interpret the Stokes profiles we must at least partially resolve the solar line profiles. We conclude that a *slit spectrograph* should be the primary instrument (a combination of slit/filter instrument might be a fruitful hybrid approach). These issues are even more critical if we are to hope to study some of the more dynamic problems (e.g. CME dynamics) discussed in section 1.1.

Thus, one should ideally try to build a magnetometer capable of measuring several ionization stages from the list given in Table 4. Preferably it should be able to observe at least two ions formed between 6.0 and 6.3 in log T_e. Given all considerations, we will try to derive a Figure of merit for each line listed in the Table, and from that list obtain a clearer picture of what an ideal coronal magnetometer based on measurements of the E-coronal emission should look like.

> **A coronal magnetometer requires:**
> • observations of lines sampling the range 6 to 6.3 in log T_e
> • spectroscopy (not filtergrams) to help understand contribution of Doppler shifts to Stokes V profiles.

3.7 Remaining instrumental considerations.

There remain several important instrumental issues that can influence the choice of lines. The relative merits of telescopes at infrared versus visible wavelengths have been clearly expounded by Beckers (1995) and Smartt and Koutchmy (1995). The scattering properties of a coronagraph objective, with a given (rough) optical surface, have been well studied. The performance improves with increasing wavelength, the scattered light intensity scaling with λ^{-2}. However, other components of an instrument have disadvantages when observing at infrared wavelengths. Detectors, cameras and polarization optics at IR wavelengths are not as readily available and not as highly developed as they are at optical wavelengths. For example, infrared array detectors typically have fewer pixels than their visible counterparts, their noise properties can deteriorate with increasing wavelength, and they are more expensive per pixel. In addition, in the thermal IR region beyond about 3 μm, significant thermal emission from the telescope, spectropolarimeter and camera system will be detrimental to the polarization signals unless the system is cryogenically cooled. For example, IR work from the NCAR C130 aircraft during the 1998 February 26 eclipse has shown that at 3.9346 μm (see Figure 3), the wavelength of the Si IX line, an instrument with an objective lens at $> 280K$, but with detectors cooled to liquid nitrogen temperatures (77K), is adequate to measure Stokes *I*. It remains unclear if thermal emission from an occulter/objective is going to be a problem for measurements of $\frac{V}{I}$ on the order of 10^{-3}.

In summary, instrumental considerations alone indicate that it is prudent to select lines as far into the infrared as possible, but ensuring that large enough detector arrays with deep wells and low read noise are available.

3.8 Magnetograph simulations of Stokes V: Figures of merit for various lines.

To assess the relative merits of the various lines we have performed simple simulations of Stokes V profiles using the magnetograph formula with no corrections for atomic alignment, and the parameters and sources listed in Table 5. Note the relatively small diameter (40cm) of the telescope used in these calculations. Figures 8 through 15 shows simulated data for the most promising lines, in order of increasing wavelength. In each figure we show the simulated intensity profile (upper panel), atmospheric transmission for a viewing angle 30 degrees to the zenith (upper middle panel), a spectral intensity atlas of the solar disk over the emission line profile, from sources listed in Table 7, and the Stokes V profile (bottom panel) computed assuming no atomic orientation or alignment (i.e. the parameter $\mathcal{K}$ is set to unity in equation 6). The integration time was 1000 s, and the LOS field strength used for computation of the V profiles was taken to be 10 Gauss. Calculations are shown for intensities computed at heliocentric

distances of $1.1R_\odot$ and $1.32R_\odot$ (left and right panels respectively)[13].

In Table 8 we list a Figure of merit for the most promising M1 lines. This Figure is simply the signal-to-noise ratio for Stokes V computed at a projected heliocentric distance of $1.1R_\odot$. In deriving this Figure no account has been taken of other issues such as the variations of detector efficiency with wavelength, availability/ efficiency/ size of detectors, cost of polarization optics, variations in telluric absorbers/scatterers with wavelength, or even lack of knowledge of the precise rest wavelength of the coronal M1 lines. Nevertheless, these Figures do represent a first attempt to rank the spectral lines- it is difficult to imagine that the ordering of the list will change much with additional information. With this in mind, inspection of the Table and Figures reveals the following results:

> - **Signal to noise ratios of 20 can in principle be attained in the best lines, low in the corona, with small aperture telescopes.**
> - **The signal-to-noise in V is highest in the lines of Fe** XIII **1.0746** μ**m and Si** IX **3.9346** μ**m.**
> - **These particular lines are also the most promising for measurements at larger projected heliocentric distances in the corona.**
> - **The effects of atmospheric absorption, while not entirely negligible, are fortunately not dominant. The only line of interest that is threatened by strong absorption is the 3.027** μ**m line of Mg** VIII. **All absorption features except Si** IX **are H$_2$O (water vapor). The absorption feature close to the Si** IX **line is from N$_2$O.**
> - **There is no need to observe lines longward of 4** μ**m.**

Table 7: Sources of solar disk spectra shown in Figs. 8 – 15.

Wavelength region μm	Type	Shorthand	Source
0.296–1.300	Flux	KFBT	Kurucz et al. (1984)
1.300–1.626	Central intensity	FTSC	Delbouille et al. (1981)
2.150–22.345	Central intensity	SL3	Farmer and Norton (1989) From *Space Lab*

---

[13]Judge (1998) stressed that the theoretical intensities used here, while of a reasonable magnitude compared with observations close to $1.1R_\odot$, fall off with increasing heliocentric distance too rapidly compared with observations, at least for the Fe XIII 1.0746 μm line. Therefore the signal to noise ratios at $1.32R_\odot$ shown in the Figures should probably be regarded as lower limits.

Table 8: Figures of Merit (Mauna Loa $D = 40$ cm at $1.1R_{\odot}$)

Ion	λ	Log I	Figure of merit	Max V/I	Log T_{e}
	μm	erg cm^{-2} s^{-1} sr^{-1}	(max s/n (V))		
Fe XIII	1.0746	1.35	23.8	5.6-4	6.22
Si IX	3.9346	-0.17	23.4	1.5-3	6.04
Si X	1.4300	0.73	11.4	4.5-4	6.13
Mg VIII	3.027	-0.36	7.2	5.6-4	5.92
Fe XIII	1.0797	0.72	6.9	2.3-4	6.22
Fe XIV	0.5303	1.36	5.8	1.5-4	6.30
Fe XI	0.7891	0.96	5.8	1.8-4	6.10
Fe X	0.6374	1.12	5.2	1.5-4	6.03
S IX	1.252	-0.07	1.7	7.2-5	6.0
Si VII	2.481	-0.71	1.1	7.0-5	5.8

Note: The values of the "Figures of Merit" are simply maxima in the signal-to-noise ratios in Stokes V: they therefore exceed the "typical" signal-to-noise ratios estimated in Section 3.2 above.
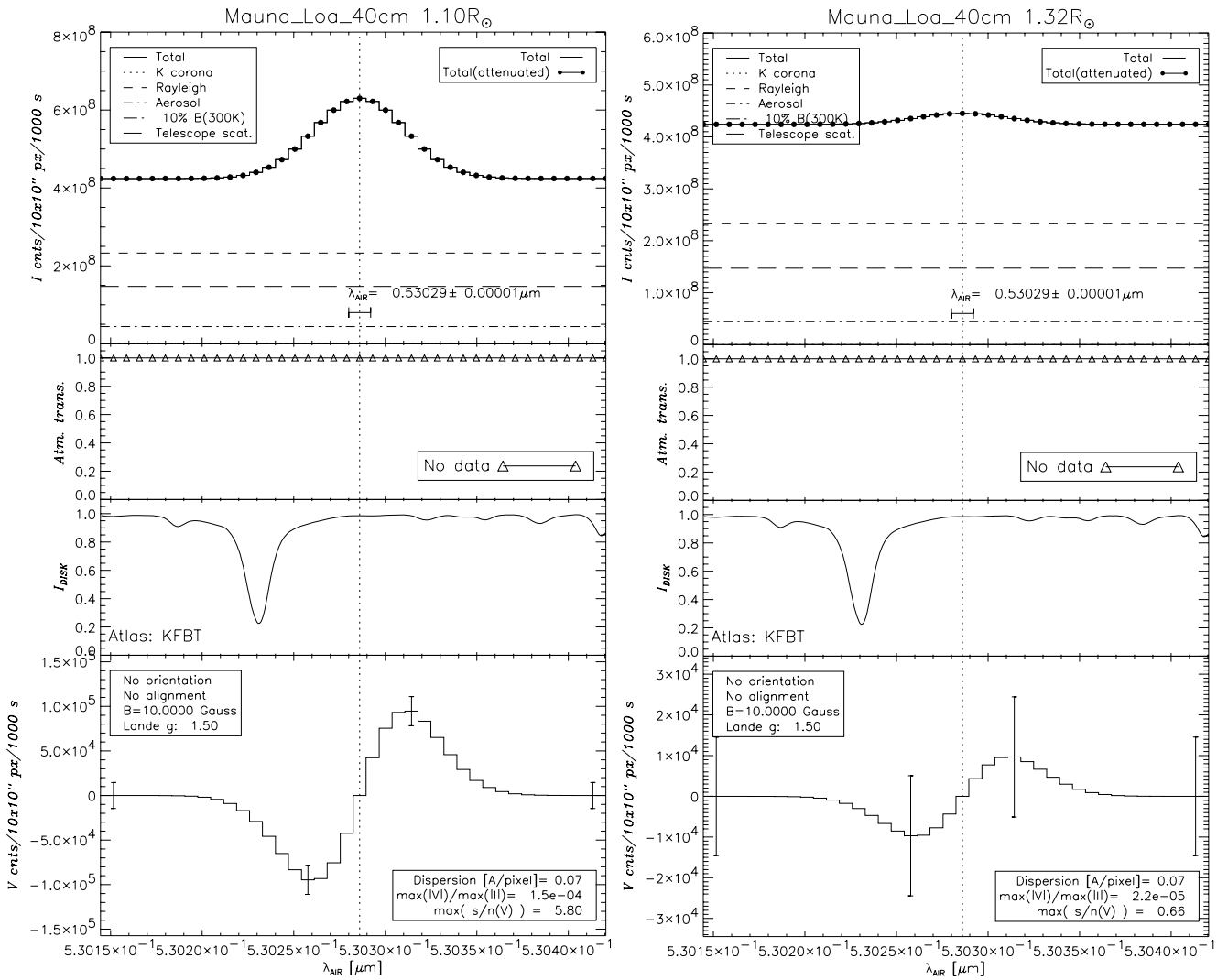
Figure 8: Synthesized *I* and *V* data, using the intensities of Judge (1998). Data are shown for Fe XIV 0.5303 μm, the Green line. No telluric absorbers are important at these wavelengths.
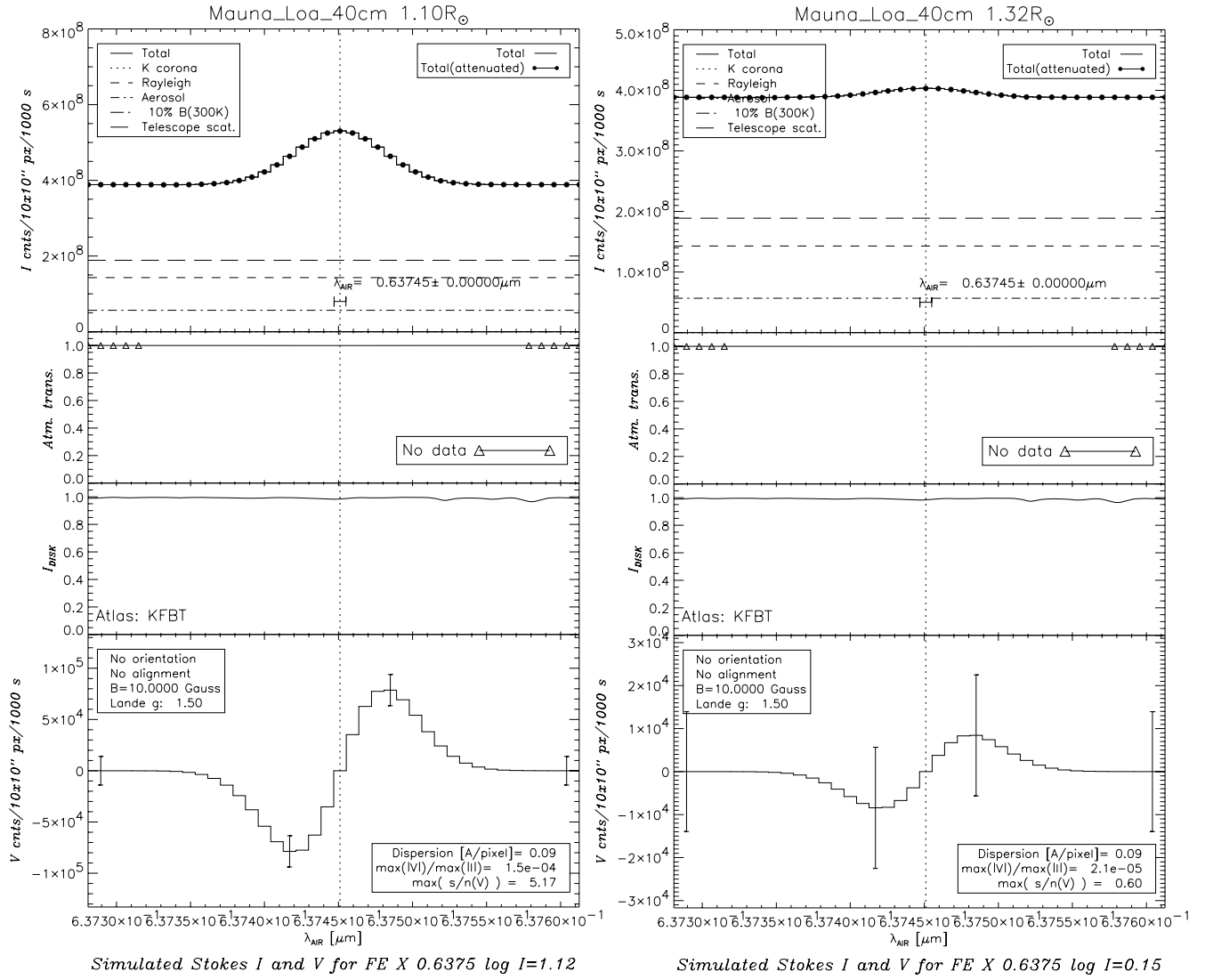
Figure 9: Synthesized *I* and *V* data, using the intensities of Judge (1998). Data are shown for Fe X 0.6374 *μ*m, the "Red line". Again, no telluric absorbers are important at these wavelengths.
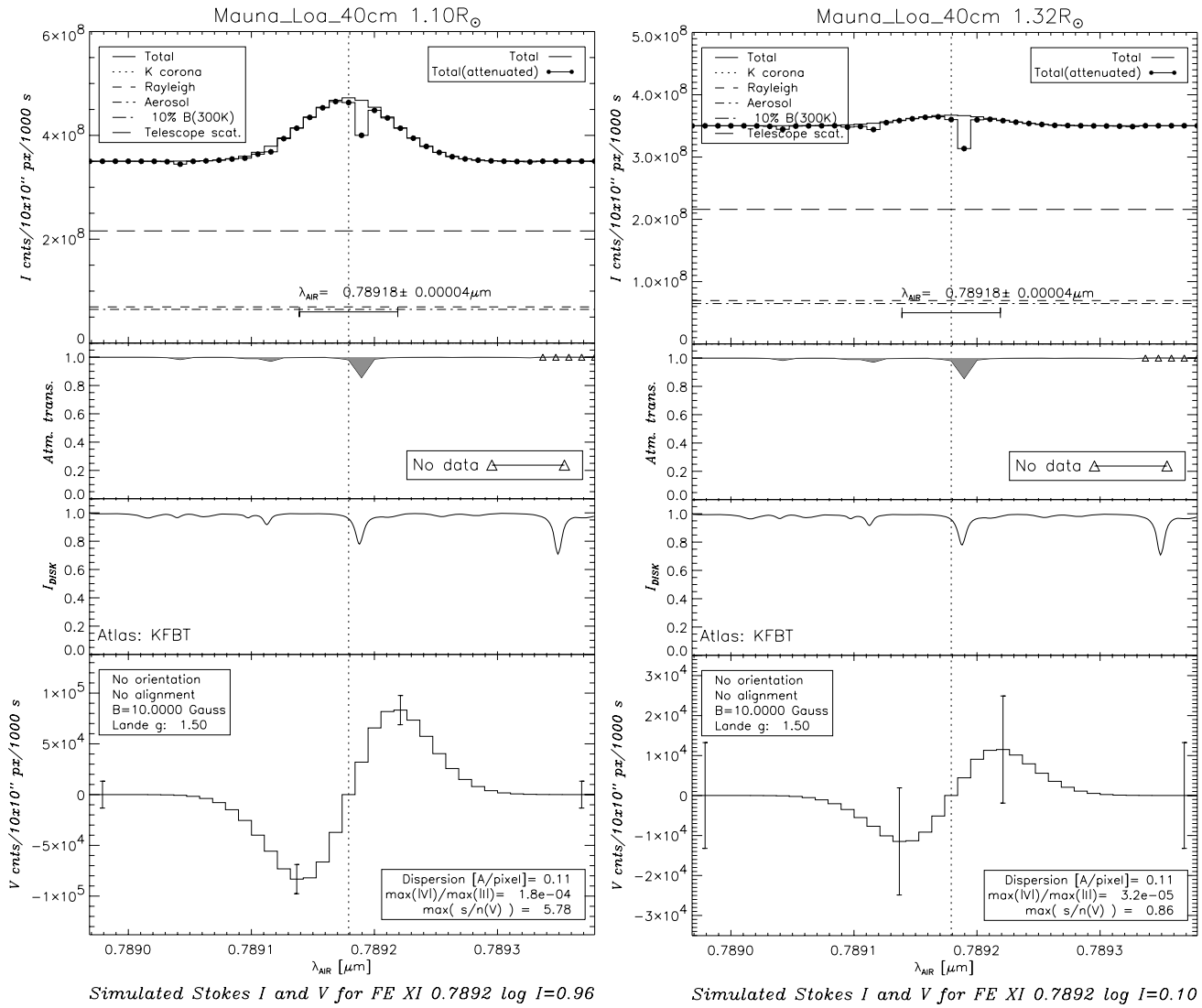
Figure 10: Synthesized *I* and *V* data, using the intensities of Judge (1998). Data are shown for Fe XI 0.7892 μm. The weak telluric absorbers are weak transitions of H_2O.
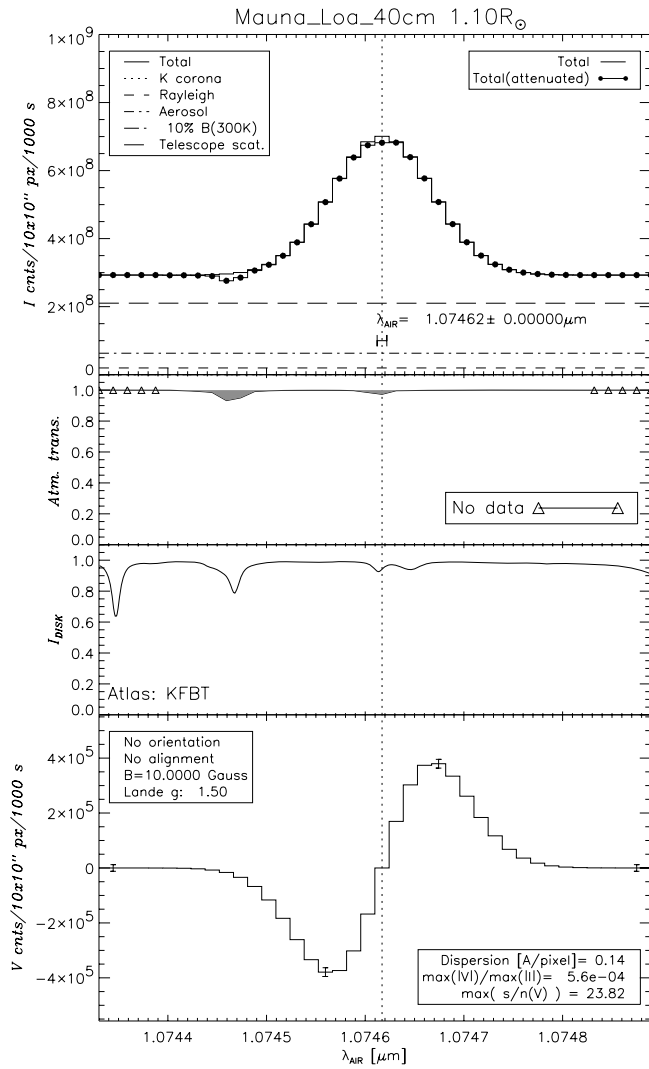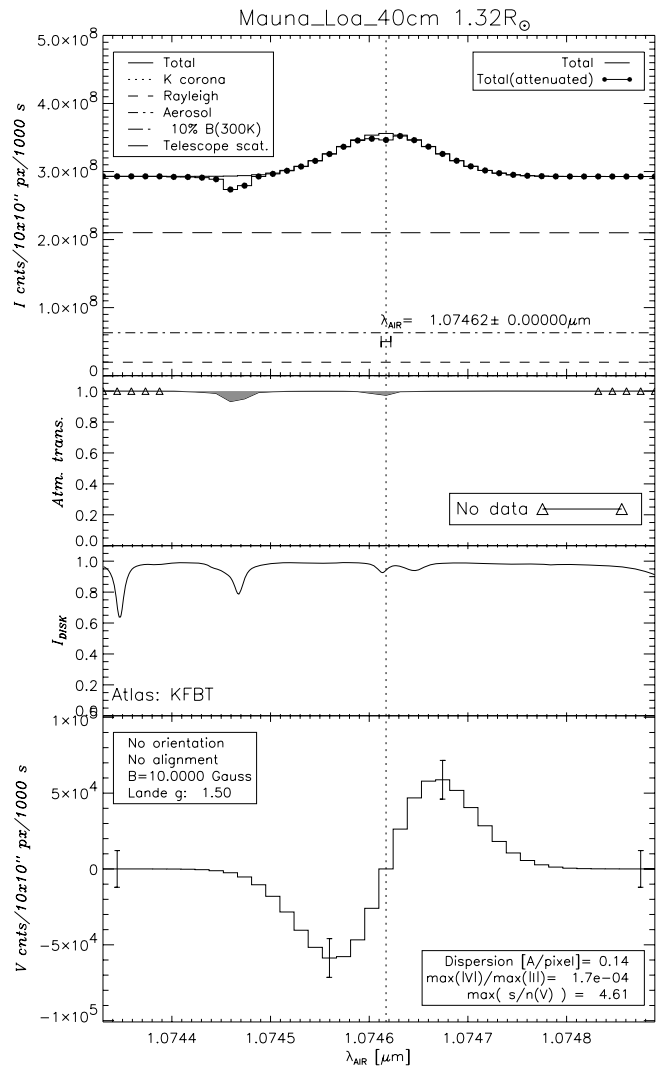
Figure 11: Synthesized *I* and *V* data, using the intensities of Judge (1998). Data are shown for Fe XIII 1.0746 μm. The weak telluric absorbers are weak transitions of H_2O.
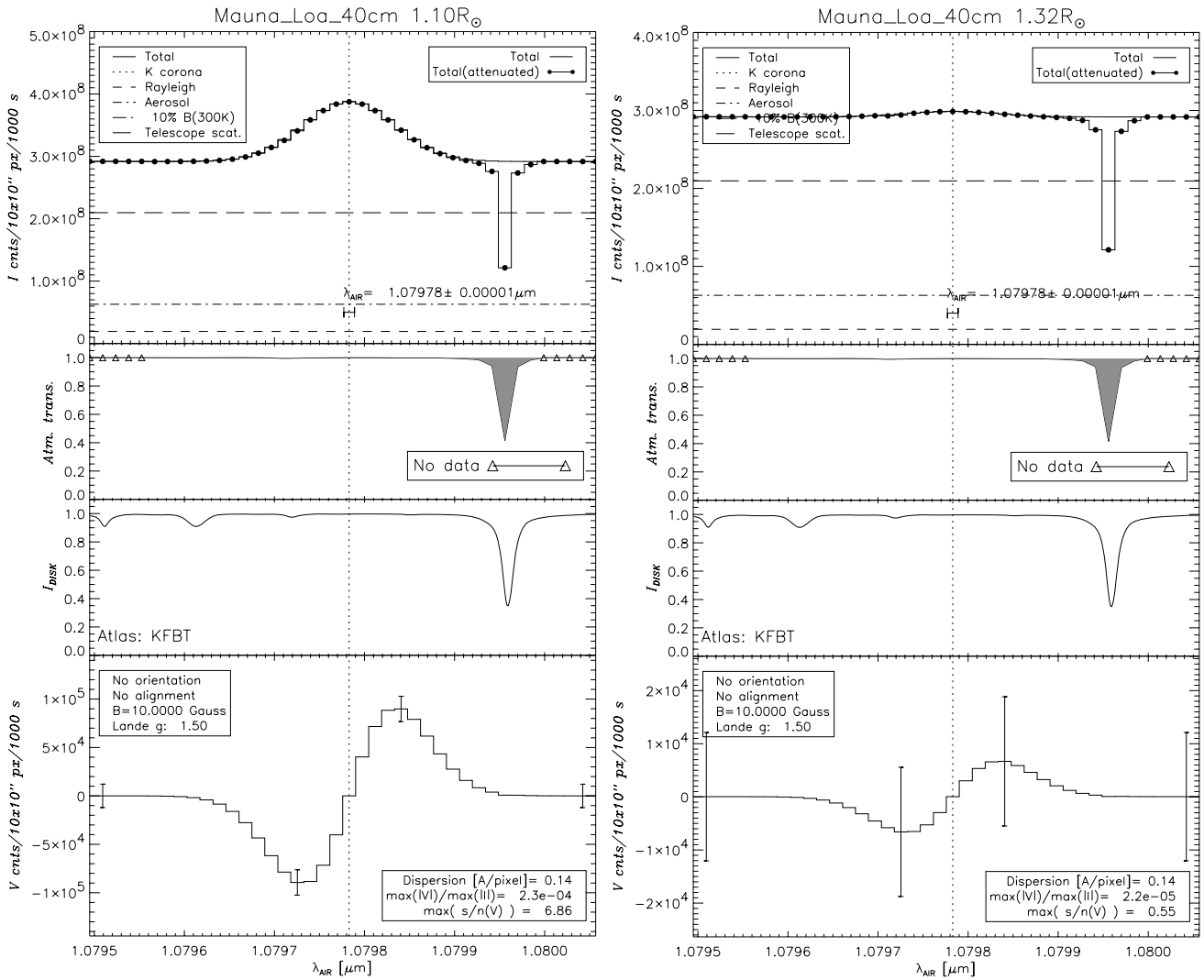
Figure 12: Synthesized *I* and *V* data, using the intensities of Judge (1998). Data are shown for Fe XIII 1.0798 μm. The telluric absorbers are transitions of H_2O.
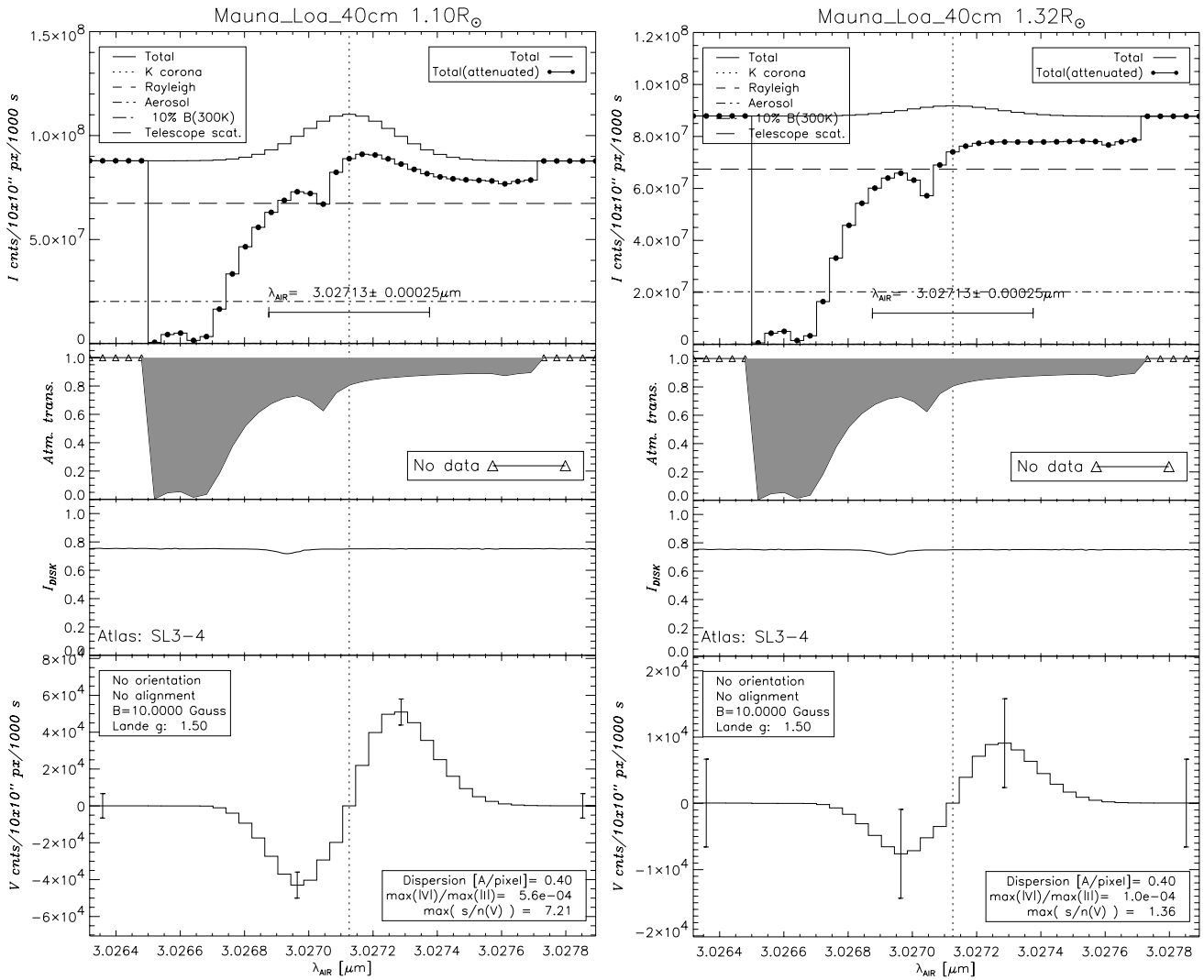
Figure 13: Synthesized *I* and *V* data, using the intensities of Judge (1998). Data are shown for Si X 1.430 μm. The telluric absorbers are transitions of H_2O.

Figure 14: Synthesized *I* and *V* data, using the intensities of Judge (1998). Data are shown for Mg VIII 3.03 μm. The telluric absorption is due to H_2O.
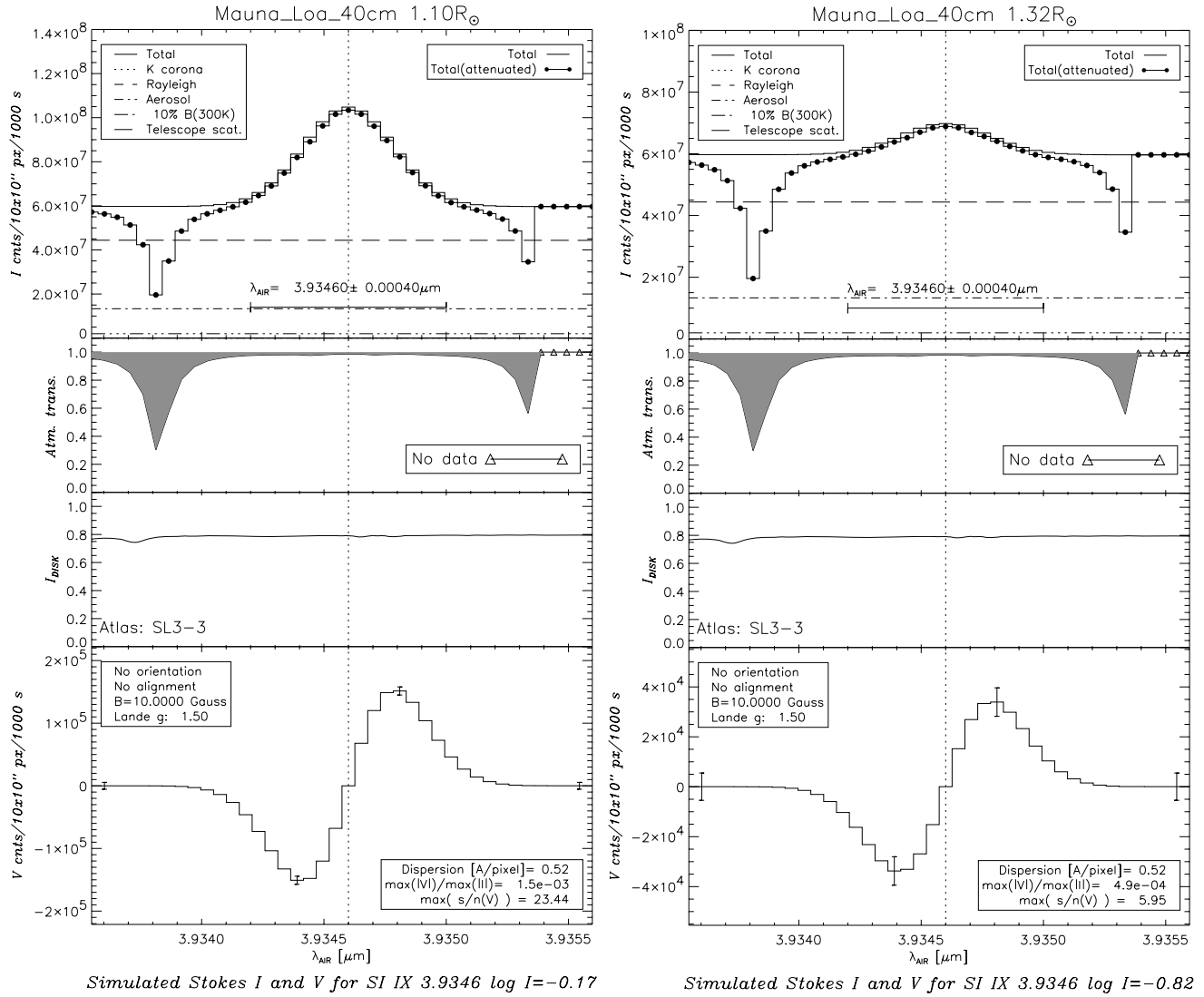
Figure 15: Synthesized *I* and *V* data, using the intensities of Judge (1998). Data are shown for Si IX 3.9346 *μ*m. The telluric absorption is due to N₂O. In this case water vapor contributes an absorption of less than 0.1%.

The Figures of merit of the various lines are shown again in figure 16, plotted as a function of wavelength and formation temperature of the lines. Some authors (e.g. Beckers 1995) have placed emphasis on developing infrared capabilities out to say 30 μm or more. While this may be of interest for other applications, there is no need to observe beyond 3.95 μm for coronal magnetometry (no strong lines exist there).

Based upon the data in these figures and Table 8, we conclude that

- **a magnetometer should be designed to observe at least the lines of Fe XIII at 1.0746 and 1.0798 μm, keeping open the possibility of observing Mg VIII at 3.027 μm Si IX at 3.9346 μm, pending their convincing detection,**
- **there is no compelling need to observe from above the earth's atmosphere, and**
- **although lines exist at longer wavelengths, they offer no advantage over those listed above because they are intrinsically weak.**
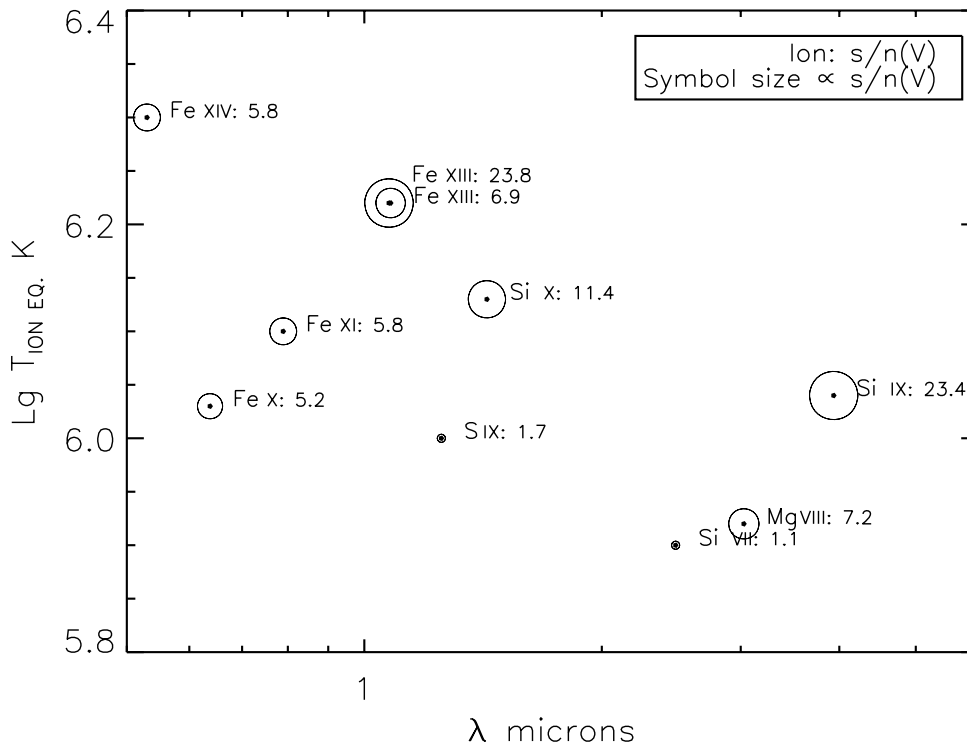
Figure 16: Merits of emission lines as a function of wavelength and formation temperature (log T), on the basis of the s/n ratio of the Stokes V profile.

3.9   Detailed simulations of Stokes I, Q, U, V for Fe XIII 1.0746

The simulations presented above were aimed at determining the magnitude of Stokes V and its observability from an observatory situated on the ground. Thus we used the magnetograph formula (accurate to a factor of 2) and focused on instrumental and atmospheric issues.

However, several important issues are not addressed by these simulations, notably the linear polarization signatures. In Section 1.1, we claimed that we could in principle determine constraints on current systems by studying the direction of the projected fields in the POS. To determine the potential for this work requires simulations that are not yet complete. Some simple potential field calculations have been done, however, that illustrate the way that three dimensional "loop" systems impart information on the magnetic field configuration into the POS Stokes profiles.

Figure 17 shows calculations of Judge and Casini (2001) based upon the formalism of Casini and Judge (1999) but which include a first approximation to collisional processes (electrons only were included so far). The field is simply generated by an inclined dipole situated at the west solar limb. Based upon images of loop systems (c.f. Figure 4), only certain "flux tubes" were loaded with plasma, mimicking the observed behavior that only certain "loops" emit much coronal emission.

The Figure confirms the expected magnitudes of linear and circular polarization. It remains to be seen whether current-carrying fields of interest to many of the problems outlined in Section 1.1 yield useful signatures of currents in the emergent Stokes parameters. Such work is under way.

3.10   Additional data needed

A close inspection of the above Figures reveals the need for a more accurate rest wavelength for the Mg VIII line at 3.027 ± 0.00025 μm (air wavelength, figure 14). It is important to determine the line's wavelength relative to the strong H_2O absorption present in the figure. The current rest wavelength is derived from measurement of the line in a photoionized astrophysical plasma (Reconditi and Oliva 1993). Similarly, it would be very useful to have a more accurate determination of the wavelength for the Si IX line at 3.9346 μm, given the presence of non-negligible absorbers close to the expected wavelength (figure 15). Currently the rest wavelength is 3.9346 ± 0.0004 μm in air, determined from active galaxy data by Oliva et al. (1994).
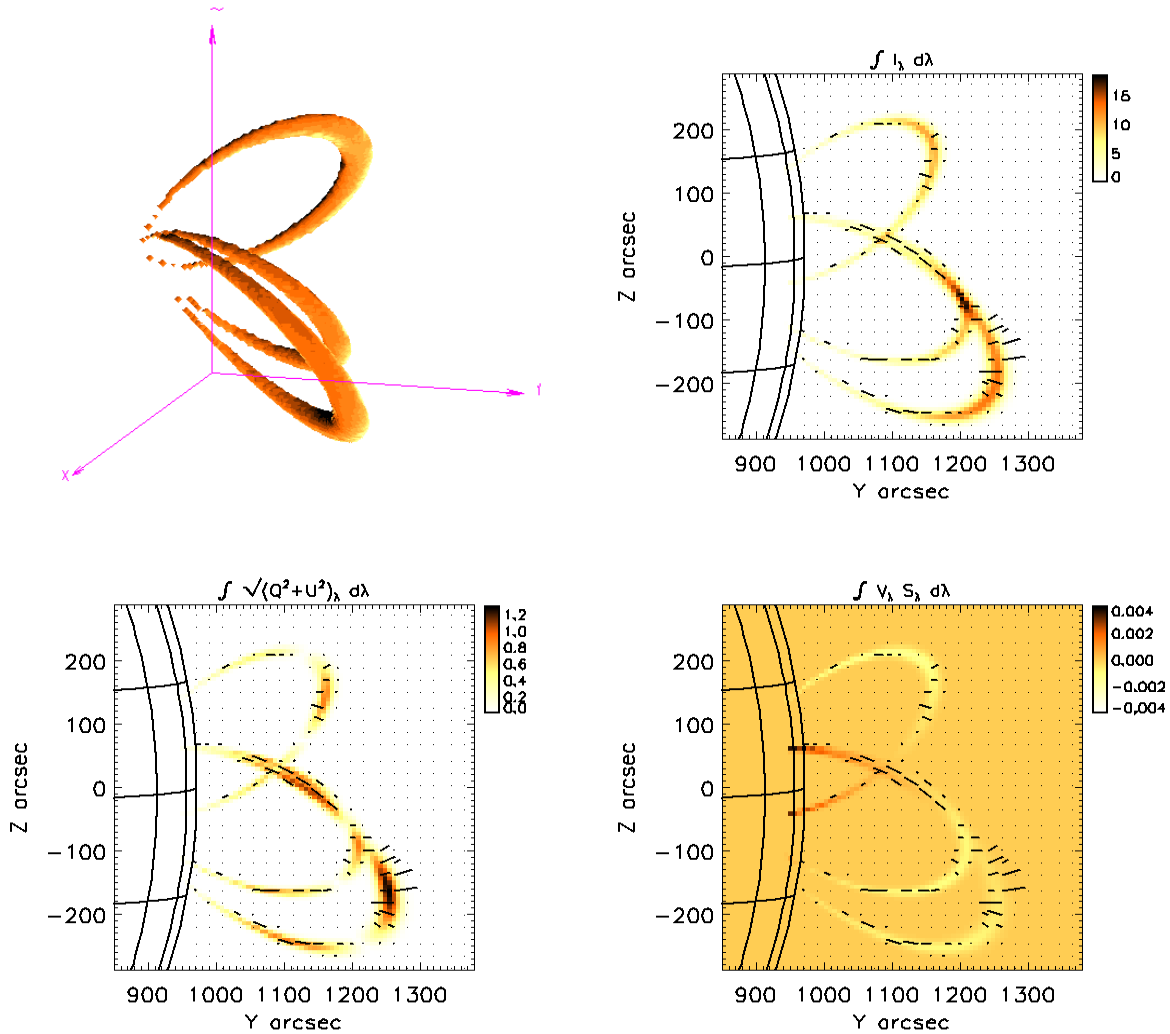
Figure 17: An example of computed polarization of the [Fe XIII] 1074.7 nm line. The top left panel shows the distribution of plasma density in "tubes" within a dipolar field. Other panels show computed Stokes data (units of erg cm^{-2} s^{-1} sr^{-1}) along the line of sight (which is the x-axis in the top left panel). S_λ used for computing Stokes V is -1 for wavelengths shortward of line center, $+1$ otherwise. The lines show the linear polarization vector (with 180° ambiguity). The calculations assumed reasonable values of field strengths (2 G at the loop tops) and thermal conditions (base electron density $N_e \approx 10^8$ cm^{-3}, $T_e \approx 2 \; 10^6$ K, 20 km s^{-1} micro-turbulence, no flows).

4   A Proposed Instrument

4.1   An "ideal" instrumental configuration

The need for observations of lines from to 1 to 4 μm provides some immediate constraints on the design of a new synoptic instrument, whether in space or on the Earth:

- The main telescope must be a reflector, preferably a coronagraph[14].

- The data must be acquired with a spectrograph (not filter system) to interpret correctly the Stokes V and I signals in terms of magnetic fields (and avoid cross talk from velocity signals).

- The detectors must have read noise much less than photon noise, and very deep wells, to be able to measure the very small Stokes V parameter close to the photon counting statistical limit, including large and variable telluric and instrumental sources of noise.

- The spectrograph (or spectrographs) and polarization optics must be able to operate at the wavelengths of the most promising lines, both near 1 and 4 μm, and be able to measure the $I + V$ and $I - V$ components simultaneously. A dual beam system is required to avoid scintillation problems.

- Critical components of the entire system (including the occulting disk) should be carefully constructed and/or cryogenically cooled to reduce thermal emission close to 4 μm. This is not a step to be taken lightly- it is a requirement for making efficient measurements longward of 3 μm.

- A field-of-view filter, "slit jaw" camera, is important for real-time context images and for studies of plasma motions.

The proposed instrument ultimately might benefit from being able to observe other lines, including the Fe XIV Green line and the 1.430 μm line of Si X observed by Penn and Kuhn (1994). It should be designed to measure the 1.0830 μm nm line of He I which potentially offers diagnosis of weak (1G) magnetic fields in any prominence material present in the LOS, via the Hanle effect, as well as LOS strength and POS field direction in the "strong field" regime expected in prominences with stronger fields.

4.2 A first step towards the "ideal" instrument

By initially restricting wavelengths to the 1 μm region, considerable simplifications to a whole system can be achieved without necessarily compromising the scientific return in the long term. Thus, we believe it makes sense to develop a focal plane instrument first with emphasis on the 1 μm region, leaving the 4 μm region until later.

The rationale behind this choice of wavelengths is as follows. First, such a focal plane instrument could be used with existing telescopes; second, a system designed to observe near 1 μm, encompassing a relatively narrow spectral range including the magnetically and density sensitive line pair Fe XIII 1.0746 1.0798 μm, can with small modifications be used to obtain Stokes profiles of the He I 1.0830 μm line. This line in principle can provide information on the *vector* magnetic field in prominence material that might be present in the instrument's field of view, through the Hanle effect, provided $|\vec{B}| \sim 1.1$ Gauss there; third, no complex cryogenic systems need be developed (other than one might consider using for the camera/ detector system); fourth, that there is considerable experience working with similar data (e.g. all the work with the KELP instrument performed in the 1970s); and last, that in fact no convincing detection of coronal lines beyond 2 μm has yet been made. While the Si IX 3.9346 μm and Mg VIII 3.027 μm lines represent *potentially* very important additional diagnostics

---

[14]It is in fact possible to observe the corona at infrared wavelengths without coronagraphic capability because of the sharp drop in photospheric scattered light intensities with increasing wavelength (J. Harvey and C. Keller 2000, private communication). Nevertheless, occulting the solar disk gives significant advantages near 1 μm.

because of their substantially lower temperature of formation (relative to Fe XIII) and high magnetic sensitivity, it must be kept in mind that the calculations shown in Figure 15 are based upon theoretical calculations, on "rest" wavelengths based on active galactic nuclei spectra, and on theoretical atmospheric transmission calculations whose transmission depends critically on knowledge of exact emission line wavelengths.

Finally, it is worth keeping in mind that an instrument dedicated to observe lines near 1 μm could also be designed to observe the Fe XIV Green line using a CCD camera (1.0746 μm is near $2 \times 0.5303 = 1.0606$ μm, for example).

5   Conclusions

In conclusion:

- We have shown that several forbidden lines exist that, with modest equipment based at a high, dry mountain site, may be used to determine new properties of the coronal magnetic field far beyond what was achievable in the 1970s, and reported in the 1980s. Space-borne instruments are not needed- atmospheric transmission is expected to be good enough for high quality work.

- We have argued that an instrument should be constructed that can observe the Fe XIII lines pair at 1.0746 and 1.0798 μm, the He I 1.0830 μm line, potentially the Green line, with an ultimate capability to measure both the Mg VIII 3.027 μm and Si IX 3.9346 μm lines. There is no need to make observations outside of this wavelength range for coronal magnetometry. The He I 1.0830 μm line can in principle be used to determine vector magnetic fields through the Hanle effect in prominence fields with $|\vec{B}| \sim 1$ Gauss, and to determine the POS field direction in the "strong field" regime in prominences with stronger field strengths.

- We have pointed out places where more data are needed. Accurate wavelengths for lines of Mg VIII and Si IX near 3.03 and 3.9346 μm respectively are needed, to 1 part in 2×10^5, to permit an accurate assessment of the potential effects of telluric absorption. A careful study of "depolarizing collisions" is needed for all strong emission lines.

- The inverse problem is so badly posed that the inverse approach must be abandoned until tomographic techniques become available. This is likely to be far in the future, if done at all. Instead, the wisest approach seems to be to combine synoptic disk observations of the photospheric field with coronal magnetometer measurements, through extrapolations.

- We have proposed that development begin with a focal plane instrument devoted to the 1 μm region, but keeping open the possibility to extend the instrumentation out to the thermal infrared at 4 μm.

A   Techniques For Measuring Coronal Magnetic Fields

The coronal magnetic field can in principle be determined in two distinct ways: direct determination using space-borne magnetometers, and indirect determination by studying the polarization signature of radiation emitted by ions (spectral lines) or electrons (Bremsstrahlung, gyroresonance) in the presence of magnetic fields. We will focus here on the indirect, remotely-sensed approach, because of obvious physical limitations inherent in the *in situ* measurements (spacecraft cannot survive below heliocentric distances of about $4R_\odot$).

Quantum mechanics tells us that the magnetic field can make its presence known, in the radiation emitted in the presence of the field, in several ways. We can make a first classification depending on whether *continuum* (free-free) or *spectral-line* (bound-bound) transitions are involved[15].

A.1   Radiative signatures of $\vec{B}$ from free-free ("continuum") transitions

In the case of *free-free* radiative transitions, i.e. those involving free initial and final states of the radiating electron, there are two physically distinct processes that lead to signatures of the magnetic field, that dominate in different regimes according to the frequency of radiation emitted and observed:

- Free electrons in a plasma permeated by a magnetic field emit radiation that can be viewed as a modified form of Bremsstrahlung radiation, at frequencies ν far away from the electron gyro-frequency, ν_e, which is $\sim 3 \times 10^7$Hz for field strengths of order 10G (Table 1). The emission becomes circularly polarized due to the differences in absorption for the ordinary and extraordinary modes of magneto-ionic theory (e.g. Dendy 1990). When observing at frequencies ν much greater than both the plasma frequency ($\nu_{pe} \approx 10^8$Hz, i.e. on the order of ν_e), the opacity in the two modes becomes a simple function of plasma density, temperature, the ratio ν/ν_e ($\gg 1$), and the cosine of the angle of the magnetic field to the LOS. Solution of the transfer equation for these modes in simple geometries yields degree of circular polarization V that is numerically

$$V(\%) = \frac{B_\parallel \,(\text{G}) \,\cdot\, \text{n} \,\cdot\, \lambda_{\text{cm}}}{107} \tag{29}$$

  where $B_\parallel$ is the longitudinal component of the field strength in Gauss, and n is the spectral index of the emergent intensity I_ν ($I_\nu \propto T_b$, the brightness temperature, in the Rayleigh-Jeans limit),

$$n = -\frac{ln\, T_b}{ln\, \nu} \; . \tag{30}$$

  $n = 2$ for an optically thin (transparent) plasma. T_b is the brightness temperature of the source), and λ_{cm} is the wavelength at which the observations are made (in cm).

- When observing at frequencies close to low harmonics of the gyro-frequency for the electrons, for example at lower frequencies for the same field strength or at the same frequencies for higher field strengths, the absorption and emission coefficients (along LOS inclined to the

---

[15]We are unaware of any way that bound-free, i.e. photoionization or photo-dissociation, transitions can yield useful information on the coronal magnetic field.

magnetic field) can enter a resonant regime[16]. This requires a moderate value for the ratio $\frac{v}{c}$ for the electrons where v is the thermal speed of the electrons– in the corona this is satisfied when $\frac{v}{c} \sim 1/30$. Thus, if the magnetic field were homogeneous, spectral "lines" of width $\frac{v}{c} \cdot s \cdot \nu_e$ would be seen in the spectrum at frequency $\nu_e \cdot s$, where s is the harmonic degree. Knowledge of s, $\frac{v}{c}$ with measurements of the radio spectrum thus yields $|\vec{B}|$ directly from the electron gyrofrequency ν_e.

The modified Bremsstrahlung technique has been successfully applied to measurements for almost four decades. For example, the RATAN-600 telescope in the Caucasus Mountains of Karachaevo-Cherkesia has produced (model-dependent, via equations 29 and 30) measurements with accuracies as low as 1-6 Gauss (e.g. Bogod and Gelfreikh 1980, Gelfreikh 1994). These measurements require high quality differential spectro-polarimetry at radio wavelengths- the levels of polarization ($|\frac{V}{I}|$) are typically small, a few percent. Furthermore, current telescopes (and those for the forseeable future) have limited spatial resolution: for example the RATAN-600 telescope has an oval-shaped beam of several arc minutes length.

The gyroresonance technique has been successfully applied to active-region observations by many authors. Recent papers have developed this area to the extent that "coronal magneto-metry" of active regions using this method is entering a phase of maturity (e.g., Brosius et al. 1997). By nature it is fundamentally limited to relatively strong magnetic fields, since the resonant frequency must exceed the frequency at which optical depth is unity in the LOS through the emitting plasma, otherwise the lines will be optically thick by the intervening Bremsstrahlung opacity. Typically it is not applicable to field strengths below 100 Gauss, and is thus of no value for typical quiet-Sun studies. This technique, in common with all remote sensing methods, suffers from fundamental ambiguities arising from the physics of spectrum formation. In the solar corona each volume element of plasma can be viewed as contributing emission at frequencies that are typically the fundamental and first 2-3 overtones at the local gyrofrequency, because the absorption and emission coefficients drop off very rapidly with increasing harmonic degree. Integrated over a finite volume of changing field strength yields emergent spectra that can be difficult to interpret[17].

In all radio observations, there is a fundamental difficulty in knowing where the "radio photosphere" (optical depth unity) occurs along the observed LOS both in the Bremsstrahlung and gyroresonant regimes. This always renders interpretation rather model dependent.

A.2 Radiative signatures of $\vec{B}$ from bound-bound ("spectral-line") transitions

Polarization in spectral lines can originate from two different mechanisms: **atomic level (Zeeman) splitting**, and **atomic polarization**. The latter, induced by anisotropic radiative or collisional processes, can be "relaxed" (i.e. partially or completely destroyed) by isotropic processes, such as impacts of particles with isotropic distribution functions, and/or radiative cascades from naturally populated levels. We highlight the physical mechanisms by which polarized light originates from atomic transitions, and later will address the specific regimes of certain kinds of

---

[16]For a field strength of 100 Gauss, derived for some active region field strengths, the gyro frequency is 2×10^9 Hz. This would be in resonance with radio waves with a wavelength of 15cm. The emission observed with e.g., the VLA or OVRO arrays is strongest at the first, second and third overtones, or at 7.5, 5, 3.75 cm respectively.

[17]Alternately, one can view the problem differently by noting that at any given observing frequency, the emergent spectrum has contributions from gyroresonant emission from typically three harmonic degrees at three different positions in the corona.

transitions of interest for determination of coronal magnetic fields. As in the main text, we follow the classification scheme outlined by Landi Degl'Innocenti (1983).

A.2.1   Radiation polarization originating from Zeeman splitting

Polarization by the Zeeman effect arises from the presence of a magnetic field in the line forming region, which separates atomic levels into magnetic sub-states. The radiation emitted in a transition between two distinct magnetic sub-states is then polarized according to the corresponding change in the magnetic quantum number, M. The polarization is made manifest in the emergent spectrum of emitted radiation through wavelength dependent polarization, because the magnetic sub-states are shifted in energy. The line transitions between them are then shifted in wavelength. Thus, the order of magnitude of the polarization (the magnitudes of Stokes Q, U and V relative to I) arising through this effect is set by the value of the parameter y where

$$y = \nu_L / \Delta\nu_D \tag{31}$$

where ν_L is the Larmor precession frequency of the atom about the magnetic field direction, and $\Delta\nu_D$ is the Doppler broadening in frequency units. The magnitudes of these parameters are:

$$\begin{aligned}
\nu_L &= \mu_B |\vec{B}|/h \tag{32}\\
&= 1.40 \times 10^6 |\vec{B}| \;\; \text{Hz}\\
\Delta\nu_D &= \nu_0 \frac{\xi}{c} \tag{33}\\
&= 10^9 \frac{\xi}{\lambda} \;\; \text{Hz,} \tag{34}
\end{aligned}$$

where e is the electron charge, m its mass, ν_0 is the frequency of the line transition, ξ is the "$1/e$" Doppler width (thermal and non-thermal contributions included) in km s^{-1} (typically 20 km s^{-1} in the corona, e.g. Tsubaki 1975), and λ the wavelength of the line transition in μm. Physically, for all cases of interest we find

$$\begin{aligned}
y &\approx 1.4 \times 10^{-3} B_\parallel \,(\text{G})\, \lambda \,(\,\mu\text{m})\, \xi^{-1} \,(\text{km s}^{-1}) \tag{35}\\
&\sim 10^{-3} \;\; \text{for } B_\parallel = 10\text{G}, \;\; \lambda = 1 \;\; \mu\text{m, and } \xi = 20 \text{ km s}^{-1}. \tag{36}
\end{aligned}$$

Furthermore, the magnitudes of transition probabilities for all M1 lines of interest are such that

$$\Delta\nu_D \gg A \tag{37}$$

where A is the radiative transition probability ("Einstein A coefficient") of the transition. As noted above, net polarization arises because the different sub-state transitions ($\Delta M = 0, \pm 1$ for example) that contribute to the line as a whole have different central wavelengths. Since the Zeeman-induced wavelength shifts are much smaller than the Doppler line widths, we can make a Taylor expansion of the the line profile in terms of the (small) parameter y. This procedure yields the well-known results:

$$\begin{aligned}
\left|\frac{Q}{I}\right| \text{ or } \left|\frac{U}{I}\right| &\propto (y \cdot \sin\theta)^2, \tag{38}\\
\left|\frac{V}{I}\right| &\propto y \cdot \cos\theta \tag{39}
\end{aligned}$$

where θ is the angle between the LOS and the magnetic field direction. Thus, in terms of Stokes I, the Stokes V parameter is first order in y, and is proportional to $\cos\theta$, i.e. the magnitude of the field strength projected along the LOS. However, Q and U are second order in y and are thus proportional to $\sin^2\theta$. Knowledge of $\sin\theta$ (from Q, U, V) then can then be used to determine the magnitude of the field strength projected onto the POS. The linear polarization $\sqrt{Q^2 + U^2}/I$ in M1 lines arising from the transverse Zeeman effect *alone* is therefore *extremely* small, and is in fact dominated by competing physical effects discussed next. For this reason, practical Stokes polarimetry of the magnetic field through use of the Zeeman effect is restricted to longitudinal (LOS) fields, through measurements of $\frac{V}{I}$.

A.2.2   Radiation polarization originating from atomic polarization

Atomic polarization results from an imbalance of populations of Zeeman sub-states pertaining to an individual atomic level, and the presence of *coherences* (quantum phase relationships) between the sub-levels themselves. The population imbalance can arise from *anisotropic and/or polarized illumination of the atom*, or from atomic collisions with particles having an anisotropic velocity distribution (*impact polarization*). In the case of emission lines formed in the (quiet-Sun) corona, the polarization of the illuminating radiation field is expected to be very small[18]. The UV/X-ray radiation originates from within the chromosphere/corona, excited by thermalized electrons, which is therefore also essentially unpolarized or very weakly polarized. Of all these processes, the *radiation anisotropy therefore plays the most important role in determining population imbalances in the radiating atom.*

Coherences arise naturally in the anisotropic and/or polarized irradiation of atomic systems where magnetic sub-levels are degenerate or quasi-degenerate. This happens when the natural widths of the sub-levels exceeds their separation, or when:

$$2\pi\nu_L \lesssim A \tag{40}$$

where A is now understood as the inverse lifetime of the level. In this case the excited levels do not evolve incoherently, but are "coupled" through the precise quantum phase relationships set by the illuminating radiation field, and must be physically described using a density matrix approach in order to track these coherences.

As a quantitative measure of the anisotropic illumination, we can use the quantity R_a/R_i, where R_a is the growth rate of the non-diagonal elements of the density matrix which appears in the statistical-equilibrium equations, and R_i is the growth rate of the diagonal elements of the density matrix (i.e. the population densities). In the absence of relaxation processes (such as collisions with thermal particles), the atomic polarization should be proportional to R_a/R_i. Then the polarization induced in spectral lines by anisotropy of the radiation field is expected to be on the order of R_a/R_i. This number can be large for some important forbidden line transitions which are irradiated by the intense, and anisotropic photospheric radiation field. The ratio R_a/R_i obviously increases with increasing distance from the photosphere.

A.2.3 $\vec{B}$ and atomic polarization: Hanle Effect (E1), resonance polarization (M1)

In the presence of both anisotropic irradiation *and* magnetic fields, the splitting of the magnetic sub-levels tends to remove their degeneracy, if it is present. Therefore, the magnetic field can

---

[18]The illuminating visible and infrared radiation originates from the almost an entire hemisphere of the photosphere, which is very weakly polarized (e.g., Stenflo and Keller 1997)

reduce or even totally destroy the coherences induced through anisotropic irradiation. The parameter determining this effect is $2\pi\nu_L/A$, where A is the Einstein coefficient for spontaneous emission of the upper level of the transition. The phenomenon of partial "relaxation" of coherences by the presence of "weak" magnetic fields ($2\pi\nu_L \lesssim A$) is known as the **Hanle effect** (e.g., Landi Degl'Innocenti 1982). In the "strong-field" regime ($2\pi\nu_L \gg A$), instead, a complete relaxation of coherences is attained, as the magnetic sub-levels are now so separated that they no longer interfere.

Note that for this "interference" effect to work, the magnetic sub-states involved must be degenerate in the sense that $2\pi\nu_L \lesssim A$. While this condition is satisfied for some allowed (electric dipole, or E1) transitions (e.g., H Ly-α) under coronal conditions, it is not satisfied at all for the forbidden lines of the "E-corona", which are magnetic dipole (M1) transitions with values of A *many* orders of magnitude smaller than for the E1 transitions. Through the Hanle effect, it can be shown that information on the vector magnetic field can be obtained. However, polarization measurements of the M1 transitions, formed away from the Hanle regime, only contain information on the direction of the magnetic field projected onto the plane of the sky (first established by Charvin 1965). This established technique (e.g., Arnaud 1982) is refered to in the text as the **resonance polarization** technique.

A.2.4   Role of particle collisions

Atomic polarization can always be affected by collisions with impacting particles (especially electrons and protons). If the particles have an isotropic velocity distribution they tend to reduce differences in the populations between magnetic sub-levels and any coherences that may exist between them. If the rate per second at which particles with isotropic velocity distribution functions impact a given sublevel is D (this rate is proportional to the density of impacting particles, page 22), the magnitude of this effect is determined by the ratio D/R_a. When combined with an isotropic component for illumination at a rate R_i as above, the polarization of spectral lines will depend on the quantity:

$$\frac{R_a}{D + R_a + R_i} \tag{41}$$

Consider, for example, the [Fe XIII] line at 1.0746 μm. Detailed calculations and observations show that $|\frac{Q}{I}|$ is of order (0.1-1) (e.g., Sahal-Bréchot 1977). The case of [Fe XIV] 0.5303 μm is similar, but has much lower linear polarization (Sahal-Bréchot 1974b) owing to considerable contributions to the sublevel populations from cascades from higher collisionally excited levels, populated "naturally" (equal sub-state populations) because the colliding particles are assumed to have an isotropic velocity distribution. Table 9 summarizes the magnitudes and scaling of the Stokes Q, U, V parameters from the various effects.

Impact polarization will not be considered further, since we will explicitly assume thermal (i.e., also isotropic) particle distribution functions.

A.3   Faraday rotation of polarized cosmic or spacecraft radio sources

Finally, there is another method: **Faraday rotation** of polarized radio sources that are seen through LOS through the corona, including spacecraft and cosmic sources. The LOS component of the magnetic field integrated through the corona can be inferred from these data (the integral of the LOS field and the electron density is the quantity actually derived from the rotation measurements). The main disadvantage of this technique is that it cannot be used for synoptic

Table 9: Magnitudes and scalings of M1 Stokes parameters

Parameter	Zeeman effect magnitude & scaling $y = \nu_L/\Delta\nu_D \sim 10^{-4}\frac{B}{[G]}\frac{\lambda}{[\mu]}$	Atomic poln. magnitude & scaling
Stokes $|Q/I|, |U/I|$	y^2	$\frac{R_a}{D+R_a+R_i}$, can approach unity†
Stokes $|\frac{V}{I}|$	y^1	$\cdots$

†Note: this parameter increases dramatically with height in the corona, because (1) collisional excitation (D) falls with the decreasing particle densities, (2) the incident radiation becomes more anisotropic.

measurements and can only provide measurements along infrequent and specific lines of sight through the corona.

A.4 Other proposals: Use of comet tails, prominences

The previous discussion reveals that there are in essence five separate ways in which components of the coronal magnetic fields may be determined in the quiet Sun: (1) modified Bremsstrahlung radiation at short radio wavelengths; (2) gyroresonance emission at longer radio wavelengths and in strong field regions (actually valid only for active Sun); (3) Faraday rotation of radio sources; (4) the Zeeman effect in various spectral lines, (5) atomic polarization induced by anisotropic irradiation of the emitting ions, and modified by the presence of the magnetic field. The Hanle effect may be considered as a (complicated) mixture of the fourth and fifth techniques to E1 lines, the "resonance scattering" effect as a relatively simple mixture of these techniques to M1 lines formed in the "strong field" regime (see the main text).

The bulk of the discussion in the main text discusses M1 lines from atomic species that are typical of the quiet Sun, e.g. Fe XIII. It is important for us to point out some possibilities using neutral atoms or singly ionized atomic species that are present at some times in the corona and and specific places. Prominences have received considerable attention in this context (e.g., Harvey 1969, Leroy 1989), and are emphasized in the main text as an important opportunity.

Less well-known is the suggestion that the gas and plasma emitted from comets might be used as a source of neutral and weakly ionized species (Kumar and Davila 1994), where one can find lines that have large sensitivities to the Zeeman effect and anomalously small Doppler widths. The novelty is that, in the solar wind, these ions don't have time to become ionized so they are unusually cool, and unusually uncharged, compared with the ions in the corona in which they are embedded. Standard Zeeman or Hanle effect might thus be applied to such lines yielding accurate determinations of the vector magnetic field. To our knowledge no such measurements have been obtained. Because these measurements can really only be done at particular orbital locations and times, such measurements can be expected to reveal only spatial and temporal snapshots of the magnetic field. While useful for some applications, these measurements could not be expected to yield by themselves answers to the questions posed in Section 1.1. Nevertheless, it is an interesting proposal that deserves the attention of nighttime observers and also coronagraphic observers, where targets of opportunity might be used to add badly needed information that is likely to be lacking in standard coronagraphic measurements. It should be taken seriously.

This proposal shows perhaps that sometimes desperation is needed to provide the ingenuity

to solve very difficult problems.

Bibliography

Amari, T., Boulmezaoud, T. Z., and Mikic, Z.: 1999, "An iterative method for the reconstruction of the solar coronal magnetic field. I. Method for regular solutions", *Astron. Astrophys.* **350**, 1051–1059

Arnaud, J.: 1982, "Observed Polarization of the Fe XIV 5303 Coronal Emission Line", *Astron. Astrophys.* **112**, 350–354

Arnaud, J. and Newkirk Jr., G.: 1987, "Mean properties of the polarization of the Fe XIII 10747Å coronal emission line", *Astron. Astrophys.* **178**, 263–268

Aschwanden, M. J., Nightingale, R. W., and Alexander, D.: 2000, "Evidence for Nonuniform Heating of Coronal Loops Inferred from Multithread Modeling of TRACE Data", *Astrophys. J.* **541**, 1059–1077

Bastian, T. S.: 1995, "Radio Diagnostics of Conditions in the Solar Atmosphere", in J. R. Kuhn and M. J. Penn (Eds.), *IR Tools for Solar Astrophysics: What's Next?*, No. 15 in National Solar Observatory/ Sacramento Peak Summer Workshop, World Scientific, Singapore, 115–126

Beckers, J. M.: 1995, "CLEAR: A Concept for a Coronagraph and a Low Emissivity Astronomical Reflector", in J. R. Kuhn and M. J. Penn (Eds.), *IR Tools for Solar Astrophysics: What's Next?*, No. 15 in National Solar Observatory/ Sacramento Peak Summer Workshop, World Scientific, Singapore, 145–161

Billings, D.: 1965, *The solar spectrum - the coronal spectrum.*, D. Reidel Publ. Co.

Bird, M. K. and Edenhofer, P.: 1990, *Physics of the Inner Heliosphere I. Large-Scale Phenomena.*, Vol. 20 of *Physics and Chemistry in Space*, Chapt. 2. Remote Sensing Observations of the Solar Corona, 13–97, Springer-Verlag, Berlin Heidelberg

Bogod, V. M. and Gelfreikh, G. B. .: 1980, "Measurements of the magnetic field and the gradient of temperature in the solar atmosphere above a flocculus using radio observations", *Solar Phys.* **67**, 29

Bommier, V. and Sahal-Bréchot, S.: 1982, "The Hanle effect of the coronal Lα line of hydrogen: theoretical investigation", *Solar Phys.* **78**, 157–178

Bray, R. J., Cram, L. E., Durrant, C. J., and Loughhead, R. E.: 1991, *Plasma Loops in the Solar Corona*, Cambridge Astrophysics Series, Cambridge University Press, Cambridge, England

Brosius, J. W., Davila, J. M., Thomas, R. J., and White, S. M.: 1997, "Coronal Magnetography of a Solar Active Region Using Coordinated SERTS and VLA Observations", *Astrophys. J.* **488**, 488–498

Burgess, A.: 1964, "Dielectronic recombination and the temperature of the solar corona", *Astrophys. J.* **139**, 776

Casini, R. and Judge, P. G.: 1999, "Spectral Lines for Polarization Measurements of The Coronal Magnetic Field. II. Consistent Theory of The Stokes Vector for Magnetic Dipole Transitions", *Astrophys. J.* **522**, 524–539

Casini, R. and Judge, P. G.: 2000, "Erratum: Spectral Lines for Polarization Measurements of The Coronal Magnetic Field. II. Consistent Theory of The Stokes Vector for Magnetic Dipole Transitions", *Astrophys. J.* **533**, 574–574

Charvin, P.: 1965, "Étude de la polarisation des raies interdites de la couronne solaire. Application au cas de la raie verte λ5303", *Ann. Astrophys.* **28**, 877

Delbouille, L., Roland, G., Brault, J. W., and Testerman, L.: 1981, *Photometric atlas of the solar spectrum from 1850 to 10000 cm^{-1}*, Kitt Peak National Observatory, Tucson, AZ

Dendy, R. O.: 1990, *Plasma Dynamics*, Oxford University Press, Oxford

Dufton, P. L. and Kingston, A. E.: 1981, "Atomic Processes in the Sun", *Adv. At. Molec. Phys.* **17**, 355–418

Dulk, G. and McLean, D.: 1978, "Coronal Magnetic Fields", *Solar Phys.* **57**, 279–295

Edlén, B.: 1943, "Die Deutung der Emissionslinien im Spektrum der Sonnenkorona", *Zeitschrift für Astrofysik* **22**, 30–64

Edwards, D. P.: 1992, *Technical Note NCAR/TN-367-STR*

Farmer, C. B. and Norton, R. H.: 1989, *A High-Resolution Atlas of the Infrared Spectrum of the Sun and the Earth Atmosphere from Space*, NASA Ref. Publ. 1224, Vol. 1

Fineschi, S., Hoover, R. B., Zukic, M., Kim, J., Walker, Arthur B. C., J., and Baker, P. C.: 1993, "Polarimetry of the HI Lyman-alpha for coronal magnetic field diagnostics", *Proc. SPIE* **1742**, 423–438

Fort, B. and Martres, M. J.: 1974, "On the Structure of the Quiet Corona near Quiescent Prominences", *Astron. Astrophys.* **33**, 249–255

Gelfreikh, G. B.: 1994, "Radio Measurements of Coronal Magnetic Fields", in V. Rusin, P. Heinzel, and J.-C. Vial (Eds.), *IAU Colloq. 144, Solar Coronal Structures*, VEDA Publishing Company, Bratislava, Slovakia, 21–28

Gibson, S. E., Biesecker, D., Guhathakurta, M., Hoeksema, J. T., Lazarus, A. J., Linker, J., Mikic, Z., Pisanko, Y., Riley, P., Steinberg, J., Strachan, L., Szabo, A., Thompson, B. J., and Zhao, X. P.: 1999, "The Three-dimensional Coronal Magnetic Field during Whole Sun Month", *Astrophys. J.* **520**, 871–879

Golub, L. and Pasachoff, J. M.: 1997, *The Solar Corona*, Cambridge Univ. Press, Cambridge UK

Grotrian, W.: 1939, *Naturwissenschaften* **27**, 214

Harvey, J. W.: 1969, *Ph.D. thesis*, University of Colorado, Boulder

Hoeksema, J. T. and Scherrer, P. H.: 1986, *The solar magnetic field- 1976 through 1985*, Technical Report UAG94, WDC

House, L. L.: 1977, "Coronal emission-line polarization from the statistical equilibrium of magnetic sublevels. I. Fe XIII.", *Astrophys. J.* **214**, 632–652

Hyder, C. L.: 1965, "The "polar crown" of filaments and the Sun's polar magnetic field", *Astrophys. J.* **141**, 1382

Judge, P. G.: 1998, "Spectral Lines for Polarization Measurements of The Coronal Magnetic Field. I. Theoretical Intensities", *Astrophys. J.* **500**, 1009–1022

Judge, P. G. and Casini, R.: 2001, "A Synthesis Code for Forbidden Coronal Lines", in M. Sigwarth (Ed.), *Advanced Solar Polarimetry- Theory, Observation, and Instrumentation*, Astronomical Society of the Pacific, San Francisco, CA

Judge, P. G., Hubeny, V., and Brown, J. C.: 1997, "Fundamental Limitations of Emission Line Spectra as Diagnostics of Plasma Temperature and Density Structure", *Astrophys. J.* **475**, 275–290

Klimchuk, J. A., Lemen, J. R., Feldman, U., Tsuneta, S., and Uchida, Y.: 1992, "Thickness variations along coronal loops observed by the Soft X-ray Telescope on Yohkoh", *Publ. Astron. Soc. Japan* **44**, L181–L185

Kohl, J. L., Noci, G., Antonucci, E., Tondello, G., Huber, M. C. E., Cranmer, S. R., Strachan, L., Panasyuk, A. V., Gardner, L. D., Romoli, M., Fineschi, S., Dobrzycka, D., Raymond, J. C., Nicolosi, P., Siegmund, O. H. W., Spadaro, D., Benna, C., Ciaravella, A., Giordano, S., Habbal, S. R., Karovska, M., Li, X., Martin, R., Michels, J. G., Modigliani, A., Naletto, G., O'Neal, R. H., Pernechele, C., Poletto, G., Smith, P. L., and Suleiman, R. M.: 1998, "UVCS/SOHO Empirical Determinations of Anisotropic Velocity Distributions in the Solar Corona", *Astrophys. J. Lett.* **501**, L127

Kuhn, J., MacQueen, R. R., Streete, J. L., Tansey, G., Hillebrand, P., Coulter, R., Lin, H., Edmunds, D., and Judge, P. G.: 1999, "Probable Discovery of a bright emission line of Si IX near 3.9 microns", *Astrophys. J.* **521**, 478–482

Kuhn, J. R.: 1995, "Infrared Coronal Magnetic Field Measurements", in J. R. Kuhn and M. J. Penn (Eds.), *IR Tools for Solar Astrophysics: What's Next?*, No. 15 in National Solar Observatory/ Sacramento Peak Summer Workshop, World Scientific, Singapore, 89–93

Kuhn, J. R., Penn, M. J., and Mann, I.: 1996, "The near infrared coronal spectrum", *Astrophys. J. Lett.* **456**, L67–L70

Kumar, C. K. and Davila, J.: 1994, "Potential IR Observations of the Solar Corona", *IAU Symposium* **154**, 81

Kurucz, R. L., Furenlid, I., Brault, J. W., and Testerman, L.: 1984, *Solar Flux Atlas from 296 to 1300 nm*, NSO Atlas Nr. 1, National Solar Observatory, Sunspot, New Mexico

Landi Degl'Innocenti, E.: 1982, "The determination of vector magnetic fields in prominences from the observations of the Stokes profiles in the D_3 line", *Solar Phys.* **79**, 291–322

Landi Degl'Innocenti, E.: 1983, "Polarization in spectral lines. II - A classification scheme for solar observations", *Solar Phys.* **85**, 32

Landi Degl'innocenti, E. and Bommier, V.: 1993, "A spectroscopic method for the solution of the 180-deg azimuth ambiguity in magnetograms", *Astrophys. J. Lett.* **411**, L49–L52

Landman, D. A.: 1975, "Proton collisional excitation in the ground configurations of Fe^{+12} and Fe^{+13} III. Transitions between magnetic sublevels", *Astron. Astrophys.* **43**, 285–290

Leroy, J. L.: 1989, "Observation of prominence magnetic fields", in *Dynamics and Structure of Quiescent Solar Prominences*, 77–113

Lin, H., Penn, M. J., and Kuhn, J. R.: 1998, "He I 10830 Angstrom line polarimetry: a new tool to probe the filament magnetic fields", *Astrophys. J.* **493**, 978

Lin, H., Penn, M. J., and Tomczyk, S.: 2000, "A new precise measurement of the coronal magnetic field strength", *Astrophys. J. Lett.* **541**, 83–86

Linker, J. A., Mikic, Z., Biesecker, D. A., Forsyth, R. J., Gibson, S. E., Lazarus, A. J., Lecinski, A., Riley, P., Szabo, A., and Thompson, B. J.: 1999, "Magnetohydrodynamic modeling of the solar corona during Whole Sun Month", *J. Geophys. Res.* **104**, 9809–9830

Longcope, D.: 1996, "Topology and Current Ribbons: A Model for Current, Reconnection and Flaring in a Complex, Evolving Corona", *Solar Phys.* **169**, 91–121

Low, B. C.: 1994, "Magnetohydrodynamic processes in the Solar Corona: Flares, coronal mass ejections, and magnetic helicity", *Phys. Plasmas* **1(5)**, 1684–1690

Low, B. C. and Lou, Y. Q.: 1990, "Modeling Solar Force-Free Magnetic Fields", *Astrophys. J.* **352**, 343–352

Lyot, B.: 1935, "Some observations of the solar corona and of prominences in 1935", *L'Astronomie* **51**, 203

Lyot, B.: 1939, "A Study of the Solar Corona and Prominences without Eclipses", *Mon. Not. R. Astron. Soc.* **99**, 580

Mariani, F. and Neubauer, F. M.: 1990, *Physics of the Inner Heliosphere I. Large-Scale Phenomena.*, Vol. 20 of *Physics and Chemistry in Space*, Chapt. 4. The Interplanetary Magnetic Field, 183–206, Springer-Verlag, Berlin Heidelberg

Marsch, E.: 1990, "Kinetic physics of the solar wind plasma", in R. Schwenn and E. Marsch (Eds.), *Physics of the Inner Heliosphere Vol II. Particles, Waves and Turbulence*, Springer-Verlag, Berlin, 45–133

Marsch, E. and Tu, C. Y.: 1997, "The effects of high-frequency Alfven waves on coronal heating and solar wind acceleration.", *Astron. Astrophys.* **319**, L17–L20

Moretto, G. and Kuhn, J. R.: 1999, "Optical design of a 6.5-m off-axis new planetary telescope", *Proc. SPIE* **3785**, 73–79

Münch, G.: 1966, "Infrared Lines of the Solar Corona I. Prediction", *Astrophys. J.* **145**, 237–241

Münch, G., Neugebauer, G., and McCammon, D.: 1967, "Infrared Lines of the Solar Corona I. Observation of [Si X] $\lambda 1.43$ μ and [Mg VIII] $\lambda 3.03$ μ", *Astrophys. J.* **149**, 681–686

Oliva, E., Salvati, M., Moorwood, A. F. M., and Marconi, A.: 1994, "Size and physical conditions of the coronal line region in a nearby Seyfert 2: the Circinus galaxy", *Astron. Astrophys.* **288**, 457–465

Olsen, K. H., Anderson, C. R., and Stewart, J. N.: 1971, "Some Newly Discovered Coronal Emission Lines from High Altitude Observations of the 7 March 1970, Solar Eclipse", *Solar Phys.* **21**, 360–371

Parker, E. N.: 1994, *Spontaneous Current Sheets in Magnetic Fields with Application to Stellar X-Rays*, International Series on Astronomy and Astrophyics, Oxford University Press, Oxford

Penn, M. J. and Kuhn, J. R.: 1994, "Ground-based detection of an infrared (Si X) coronal emission line and improved wavelengths for the infrared (Fe XIII) emission lines", *Astrophys. J.* **434**, 807

Penn, M. J., Kuhn, J. R., Arnaud, J., Mickey, D. L., and Labonte, B. J.: 1994, "Coronal Electron density measurements using the near-IR [Fe XIII] emission lines", *Space Sci. Rev.* **70**, 185

Perche, J. C.: 1965, *C. R. Acad. Sci. Paris* **260**, 6036

Perche, J. C.: 1965, *C. R. Acad. Sci. Paris* **261**, 5319

Pneuman, G. and Kopp, R.: 1971, "Gas-magnetic field interactions in the solar corona.", *Sol. Phys.* **18**, 258–270

Querfeld, C.: 1977, "A near-infrared coronal emission-line polarimeter.", *SPIE 122, Optical Polarimetry–Instrumentation and Applications* 200–208

Querfeld, C. W. and Smartt, R. N.: 1984, "Comparison of coronal emission-line structure and polarization.", *Sol. Phys.* **91**, 299–310

Reconditi, M. and Oliva, E.: 1993, "Accurate Wavelengths of Near Infrared Coronal Lines From Spectroscopic Measurements of NGC6302", *Astron. Astrophys.* **274**, 662

Rothman, L. S.: 1992, *JQSRT* **48**, 469–507

Sahal-Bréchot, S., Malinovsky, M., and Bommier, V.: 1986, "The polarization of the O VI 1032 Å line as a probe for measuring the coronal magnetic field via the Hanle effect", *Astron. Astrophys.* **168**, 284–300

Sahal-Bréchot, S.: 1974a, "Role of collisions in the polarization degree of the forbidden emission lines in the solar corona I. Depolarization by proton impact. Application to the green line of Fe XIV and to the Infrared Lines of Fe XIII", *Astron. Astrophys.* **32**, 147–154

Sahal-Bréchot, S.: 1974b, "Role of collisions in the polarization degree of the forbidden emission lines in the solar corona II. Depolarization by electron impact and Calculation of the polarization degree of the green line of Fe XIV", *Astron. Astrophys.* **36**, 355–363

Sahal-Bréchot, S.: 1977, "Calculation of the polarization degree of the infrared lines of Fe XIII in the solar corona", *Astrophys. J.* **213**, 887–899

Schrijver, C. J. and Harvey, K. L.: 1994, "The photospheric magnetic flux budget", *Solar Phys.* **150**, 1

Shurcliff, W. A.: 1962, *Polarized Light*, Harvard Univ. Press, Cambridge, Mass

Smartt, R. N. and Koutchmy, S.: 1995, "Reflecting Coronagraphs: Prospects", in J. R. Kuhn and M. J. Penn (Eds.), *IR Tools for Solar Astrophysics: What's Next?*, No. 15 in National

Solar Observatory/ Sacramento Peak Summer Workshop, World Scientific, Singapore, 163–173

Stenflo, J. and Keller, C.: 1997, "The second solar spectrum. A new window for diagnostics of the Sun.", *Astron. Astrophys.* **321**, 927–934

Stix, M.: 1989, *The Sun. An Introduction*, Springer, Berlin

Swings, P.: 1944, "Suggestions for infrared observations of the solar corona", *Publ. Astron. Soc. Pac.* **56**, 80

Tsubaki , T.: 1975, "Line profile analysis of a coronal formation observed near a quiesent prominence: intensities, temperatures and velocity fields", *Solar Phys.* **43**, 147–175

White, S.: 2001, "Solar Coronal Magnetic Fields", in G. Mathys, S. Solanki, and D. Wickramasinghe (Eds.), *Magnetic Fields Across the Hertzsprung-Russell Diagram*, Procs. International Inter-Institutional Workshop, ASP Conf. Ser., in press

Index